Geoscience Frontiers 17 (2026) 102286

Contents lists available at ScienceDirect

Geoscience Frontiers

journal homepage: www.elsevier.com/locate/gsf

Research Paper

Rethinking unconventional groundwater resources from continental shelves: Insights from the Po-Adriatic system

Bruno Campo [a,*], Marco Antonellini [a], Claudio Pellegrini [b]

[a] Department of Biological, Geological and Environmental Sciences (BiGeA), University of Bologna, Piazza di Porta San Donato 1, 40126 Bologna, Italy
[b] National Research Council (CNR), Institute of Marine Science (ISMAR), Via Gobetti 101, 40129 Bologna, Italy

ARTICLE INFO

Article history:
Received 26 August 2025
Revised 22 January 2026
Accepted 19 February 2026
Available online 20 February 2026

Keywords:
Unconventional groundwater resources
Sustainability
Open-source data
High-resolution stratigraphy
Hydrogeological modelling
Climate change adaptation

ABSTRACT

Offshore freshwater resources hosted within continental shelves constitute a valuable resource for coastal regions experiencing increasing water scarcity. This study identifies and characterizes significant fresh and brackish groundwater resources within the Western Mediterranean by integrating and reinterpreting multi-proxy datasets available from public repositories. Onshore-offshore correlation of well logs revealed laterally continuous gravel and sand bodies, with resistivity locally exceeding 30 Ω·m, indicative of fresh water within the uppermost 300 m beneath the northern Adriatic seabed. These permeable bodies are part of the Pleistocene (last 870 kyr), multi-layered succession composed of vertically-stacked aquifers and aquitards/aquicludes deposited in fluvio-deltaic, coastal, and shelfal environments. A conservative volumetric assessment indicates approximately 26.5 km^3 of fresh water (>15 Ω·m) within ~35 km of the modern shoreline, with an additional ~33.4 km^3 of brackish water (<15–5 Ω·m) extending ~15 km further offshore and reaching depths of ~500 m below the seabed. The stratigraphic architecture, governed by tectonic activity and glacio-eustatic oscillations, primarily control the geometry, distribution, and connectivity of these offshore aquifers. Integration of stratigraphic reconstructions with hydrogeological modelling indicates that several offshore aquifers are hydraulically connected to inland systems, implying active recharge and potential renewability.

This study demonstrates how geological methodologies originally developed for hydrocarbon exploration can be effectively repurposed to identify offshore groundwater, quantify volumes, and distinguish renewable from non-renewable aquifer systems. Furthermore, the systematic reuse of existing datasets provides an efficient, low-impact, and cost-effective strategy for preliminary offshore groundwater investigations across continental shelves worldwide.

1. Introduction

Severe and long droughts are increasingly striking Europe (Toreti et al., 2023), including the Western Mediterranean, where dry periods have historically occurred less frequently (Bonaldo et al., 2023). According to future scenarios, dry conditions could become the norm at these latitudes (Levantesi, 2022), with high risk of dramatic water shortage (Spano et al., 2021), especially along the coastal zones. Here, climate change effects are further reducing already limited freshwater reserves (Custodio, 2002; UN-water, 2020), which are already overexploited and generally compromised by seawater intrusion (Custodio, 2010) due to sea-level rise (Zamrsky et al., 2024a) and subsidence (Teatini et al., 2011), as well as by extreme flood events (Valente et al., 2025).

In this framework, Offshore Fresh Groundwater (OFG) stored in shelf deposits may represent an unconventional and strategic source of water to alleviate forthcoming water crises (Bakken et al., 2012). OFG is characterized by a Total Dissolved Solids (TDS) concentration below that of seawater (about 35,000 mg/L) and, because of its large distribution, is already considered "a global phenomenon" (Post et al., 2013). Globally, approximately 73% of OFG is stored in siliciclastic aquifers on passive margins, mostly in shallow waters (<100 m depth) and within 55 km of the coastline (Micallef et al., 2021). For these reasons, continental shelves are the most important hubs for OFG exploration, as also proven by the IODP Expedition 501 "New England Shelf Hydrogeology", which aims to acquire new core data to characterize the OFG bodies of the North Atlantic shelf. As a matter of fact, the

* Corresponding author.
E-mail addresses: bruno.campo@unibo.it (B. Campo), m.antonellini@unibo.it (M. Antonellini), claudio.pellegrini@bo.ismar.cnr.it (C. Pellegrini).

https://doi.org/10.1016/j.gsf.2026.102286

majority of OFG documentation relies upon geophysical data such as resistivity logs which indirectly indicate salinity or TDS (Attias et al., 2021; Haroon et al., 2021). Most discoveries of potential OFG reserves were made incidentally during hydrocarbon exploration or deep-sea drilling operations (Hathaway et al., 1979; Mountain et al., 2009; Lofi et al., 2013a; van Geldern et al., 2013; Gustafson et al., 2019; Micallef et al., 2020) with very few exceptions, as the recent Pearl River Delta investigation (Sheng et al., 2023). Due to the limited offshore borehole coverage (Lofi et al., 2013b; Jiao et al., 2015), direct observations of offshore aquifers, their structure and geochemical characteristics are rare, and still several gaps in knowledge need to be assessed, like the control exerted by the stratigraphic setting and how the evolution of continental shelves during multiple sea-level cycles affect the emplacement and dynamics of OFG (Micallef et al., 2021; Person et al., 2025). Therefore, distribution, extent and dimension of OFG bodies require further investigation, as well as mechanisms and timing of their emplacement. Furthermore, given that sustainable groundwater exploitation is feasible only in aquifer systems characterized by active recharge, priority should be accorded to the identification and assessment of such systems (Campo et al., 2024). Considering the large volumes of OFG in continental shelves (Zamrsky et al., 2022), this study aims to answer some of these questions through the high-resolution hydrostratigraphic reconstruction of the Pleistocene-Holocene succession along coastal-to-shelf transects of the Po-Adriatic system. Given its physiographic framework between two active orogens and the large availability of subsurface data (Fig. 1), this system is a promising area to identify OFG resources that may be sustainable due to their potential connection with recharging areas upstream (Regione Emilia-Romagna and Eni-Agip, 1998). In addition, the existence of freshwater reserves in the study area has been informally reported in the "*Isola delle Rose*" case (Angrilli, 2024). Furthermore, the well-constrained geological framework derived from decades of subsurface investigations (Dondi and D'Andrea, 1986; Dalla et al., 1992; Ori, 1993; Scardia et al., 2006; Ghielmi et al., 2010; Garzanti et al., 2011; Rossi et al., 2015; Zecchin et al., 2017, 2022) provides an ideal basis for disentangling the relative roles of tectonics and glacio-eustatic oscillations on the distribution and emplacement of OFG. However, in spite of the high-resolution hydrostratigraphic reconstruction carried out in the Po Plain (i.e., onshore sector — Regione Emilia-Romagna and Eni-Agip, 1998; Regione Lombardia and Eni-Divisione Agip, 2002) and the well-data from offshore locations (Fig. 1), the basinward continuity of the onshore aquifer systems has received far less attention. A first attempt to reconstruct the offshore continuity of onshore aquifers was carried out in the northern sector of the Adriatic Sea, but no freshwater was identified (Giustiniani et al., 2022). Based on coastal-to-shelf well logs correlation, the preliminary hydrostratigraphic reconstruction by Campo and Antonellini (2024) showed that the uppermost Middle-Upper Pleistocene interval of the northern Adriatic shelf locally exhibits high-resistivity values, which may reflect the presence of freshwater. A subset of these logs has recently been integrated into a dedicated database aiming at advancing OFG investigations (Giustiniani et al., 2022), revealing scattered aquifer bodies with salinity below 25,000 mg/L and further supporting the selection of the study area as key sector for OFG exploration.

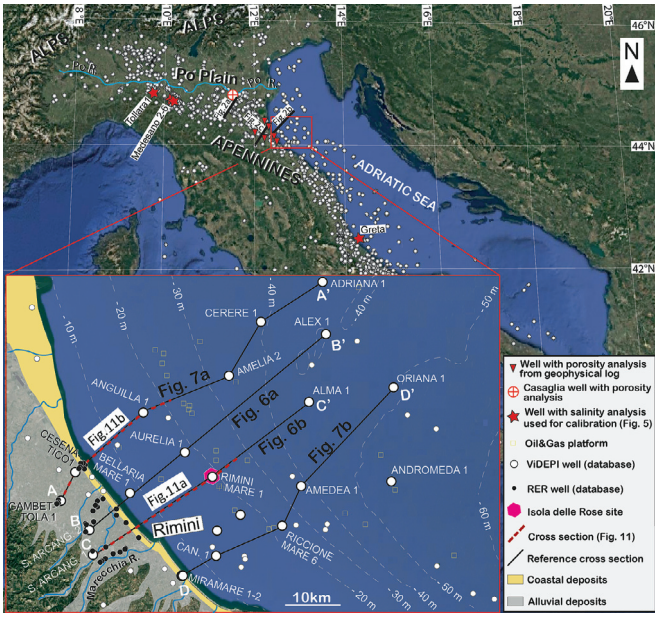

Fig. 1. Study area and dataset distribution. Map showing the spatial extent of the study area, the location of wells from the ViDEPI and Regione Emilia-Romagna Geological Survey, and the traces of the seismic profiles (Fig. 2a-b), and hydrostratigraphic cross-sections (Figs. 2c, 6, 7 and 11). Coastal and alluvial deposits of the modern coastal plain are also shown (modified after Bertolini et al. (2008)). RER: Regione Emilia-Romagna Geological Survey. Po R.: Po River.

The reinterpretation of legacy subsurface data represents a valuable resource for groundwater investigations and aquifer characterization. Recent studies have demonstrated its effectiveness, notably through the identification of freshened groundwater bodies underneath the carbonatic Hyblean Plateau (Lipparini et al., 2023) and their offshore extension up to 10 km from the coastline (Chiacchieri et al., 2025).

This research, entirely based on the reinterpretation of open-source data, provides the first identification of extensive OFG reserves on the Western Mediterranean shelf, highlighting the roles of tectonics, glacio-eustasy, and the utility of open-access datasets in guiding OFG exploration. Key aims include reconstructing the aquifer systems from onshore recharge zones to the offshore Adriatic shelf, classifying apparent resistivity values linked to pore-water salinity, and identifying Pleistocene aquifer units and defining their geometry and spatial relationships. The study also involves mapping aquifers' thickness, estimating fresh and brackish water volumes, and developing a preliminary hydrogeological model to assess resource sustainability and recharge potential.

2. Study area

2.1. Geographic and physiographic setting

The study area, approximately 2500 km^2, is located in the southernmost sector of the Po Plain (Northern Italy), in proximity to the Apennine margin, and extends from the coastal plain to about 55 km off the Emilia-Romagna coast (Fig. 1). The Po Plain watershed, about 74,500 km^2, is encased between the Alps to the north and Apennines to the south (Fig. 1). About half of the Po Plain is below 50 m in elevation, whereas 30,790 km^2 lie above 200 m (Correggiari et al., 2005). The Po River is the longest river in Italy (652 km), and flows into the Adriatic Sea, crossing the Po Plain from west to east (Fig. 1). The Po River represents a trunk river acting as a major conveyor belt for the sediment delivered by its Alpine and Apennines tributaries. The Alpine rivers generally flow through former glacial valleys and have high discharges due to snow melt. On the other hand, the Apennine tributaries are characterized by a short stretch of high-altitude reach and have a lower course with low gradients. Because of the higher erodibility of Apennine lithologies and the lack of depositional area upstream of the junction with the Po River, Apennine rivers supply larger amounts of sediment than Alpine ones (Cattaneo et al., 2003). The mean annual rainfall over the Po watershed is 1107 mm

(Correggiari et al., 2005). The onshore part of the study area is included within the alluvial fan system of the southern Apennine margin (Amorosi et al., 1996; Nesci et al., 2010), where the Marecchia River has developed the widest alluvial fan in the area (Fig. 1; Severi et al., 2014). This sector is characterized by a higher topographic gradient than the northern coastal area, with mean elevations ranging between 2 and 10 m above sea level (Perini and Calabrese, 2010). The offshore portion is part of the shallow (0–50 m depth) and gently dipping shelf (about 0.02°; Cattaneo et al., 2007) of the northern Adriatic Sea. The latter is a narrow epicontinental basin, elongated for 800 km NW-SE and 200 km across, and represents the distal portion of the Po Basin (Fig. 1).

2.2. Geological and tectonic framework

The Po Plain-Adriatic Sea system is part of the Alpine-Apennine foreland basin (Fig. 1; Amorosi et al., 2016). The tectonic setting is considered active because the south-verging Southern Alps and the north-verging Apennines form two opposing fold-and-thrust belts that initiated in the Cretaceous, because of the collision between the European Plate and the Adria microplate (Carminati and Doglioni, 2012). According to these authors, the Alps and the Apennines formed along opposite-facing subduction zones, which inverted the former Tethyan passive continental margins located at the boundaries between the European, African and Adriatic plates. The subsequent Cenozoic compressional phase affected the area at different times and with changing directions of tectonic movement: the Southern Alps system (N-S compression) during Middle Eocene to Miocene; and the Apennine system (NNE-SSW compression) from Oligocene to Plio-Pleistocene (Ghielmi et al., 2013). The Northern Apennines foreland evolved through successive tectonic phases, producing a stepwise outward migration of the thrust-and-fold belt. This process generated a series of migrating, asymmetric foredeeps (Ricci Lucchi, 1986) and associated piggyback basins developed on the inner side of advancing thrust sheets (Ori and Friend, 1984). The most external part of the two accretionary wedges is buried beneath the Po Plain and the north Adriatic Sea (Amadori et al., 2019). In the eastern sector of the Po Plain-Adriatic system, where the study area is located, the buried structures of the Northern Apennines (Fig. 2a-b) consist of different arched thrust systems, with convexity towards the NNE (Ghielmi et al., 2013). These thrust systems are active since the Late Miocene (Boccaletti et al., 2011; Petracchini et al., 2025). The combination of high subsidence rates (about 2.5 mm/yr; Carminati et al., 2003) and large volumes of sediment supplied by the orogens (Ghielmi et al., 2013) caused the accumulation of up to 8-km-thick Plio-Quaternary deposits along the foreland basin (Fig. 2a; Pieri and Groppi, 1981; Cattaneo et al., 2003). This sedimentary succession fills a wedge-shaped basin with the deepest part of the wedge bordering the thrust front (Regione Emilia-Romagna and Eni-Agip, 1998), and displays an asymmetric configuration, with major depocenters generally shifted toward the Apennines (Ghielmi et al., 2010). Tectonic activity progressively shaped the basin configuration and caused the formation of six distinct (A, B, D, E, F and G) sequence-bounding unconformities (Fig. 2a). The two youngest F and G unconformities have been dated approximately 870 kyr BP (Muttoni et al., 2003) and 450 kyr BP, respectively. Their origin has been linked to the two most recent uplift episodes of the Apennines (Regione Emilia-Romagna and Eni-Agip, 1998). They also correspond to periods of global and regional physiographic changes driven to eustasy (Ridente et al., 2008; Clark et al., 2024).

2.3. Stratigraphic architecture

The Plio-Quaternary Po Plain-Adriatic sedimentary fill is composed of siliciclastic deposits that show a general shallowing-upward trend, from deep-marine turbidites (Pliocene and Early Pleistocene), to shelf, coastal-deltaic and alluvial strata (Mid-Late Pleistocene and Holocene), reflecting the gradual filling of the basin (Bruno et al., 2024). The F unconformity marks the boundary between the uppermost Quaternary marine cycle Qm_3, including shallow-marine to deltaic deposits, and the overlying Po Supersynthem (Fig. 2a). The latter is mainly composed of Middle Pleistocene-to-Holocene continental deposits, and the recognition of the G unconformity allowed its further subdivision into Lower and Upper Po Synthems (Fig. 2a; Amorosi and Pavesi, 2010). Recently, the six unconformities (and associated sequences) were mapped throughout the Po Basin and the North Adriatic shelf, and renamed as shown in Fig. 2b (after Ghielmi et al., 2013; Amadori et al., 2019). The PS3 unconformity (PS3u) is equivalent to surface F, and the Po Supersynthem constitutes the alluvial portion of the PS3s (Bruno et al., 2024). In proximity of the foredeep, at the easternmost portion of the study area, the PS3u marks the sharp depositional change from turbidites of the older PS2s to the overlying sand-lobe deposits of the PS3s (Ghielmi et al., 2010). Deep-water sedimentation was restricted to the foredeep and locally to the ramp and foreland areas. In contrast, alluvial (fluvial and floodplain), deltaic, coastal, shelf, and slope deposits were widely distributed across the study area (Ghielmi et al., 2013). Here, PS3s displays an overall regressive trend and is characterized by the progradational geometries of the Apennine Complex and the Po Plain Complex, prograding toward NE and SE, respectively (Fig. 2b; Ghielmi et al., 2013). PS3s is approximately 1000 m thick (Fig. 2b), and consists of a lower interval of slope, shelf, coastal, and deltaic deposits, overlain by an upper interval of alternating continental, coastal/deltaic, and shallow-marine strata. Landward, PS3s reaches up to 800 m in thickness and wedges out toward the Apennine margin, where the stratigraphic architecture is characterized by amalgamated alluvial-fan bodies passing downdip into alternating fluvial-channel sands, overbank muds, and coastal deposits (Fig. 2c; after Amorosi and Colalongo, 2005). Well-log analysis and stratigraphic correlation indicate that PS3s records a climate- and eustasy-driven cyclicity, expressed by the alternation of thick sand-bodies and muddy intervals deposited during lowstand and highstand phases, respectively (Ghielmi et al., 2013).

2.4. Sea-level oscillations and palaegeography

Similarly to other Quaternary continental margins worldwide, long-term climate fluctuations with a periodicity of about 100 kyr controlled the evolution of the Po-Adriatic system over the past 800 kyr (Amorosi and Pavesi, 2010; Lobo and Ridente, 2014). In response to glacio-eustatic forcing, the Po River Delta repeatedly shifted landward and seaward during the Middle-Late Pleistocene (Amorosi et al., 2016), leading to the development of extensive alluvial and delta plains during glacial lowstands (Maselli et al., 2011) that were drowned during subsequent sea-level rise events (Storms et al., 2008; Pellegrini et al., 2015). This cyclic migration of the Po Delta and associated coastal systems progressively shaped the modern North Adriatic shelf (Zecchin et al., 2017). During the Last Glacial Maximum (about 26 kyr BP; Clark et al., 2009), sea-level dropped to about 135 m below its present level (Lambeck et al., 2014) and extensive glaciers capped the Alps (Monegato et al., 2007). As a consequence, the Po River catchment nearly doubled, and the largely exposed North Adriatic shelf was transformed into a fully alluvial plain across which the Po River flowed (Pellegrini et al., 2018).

The identification of eight transgressive–regressive (T-R) successions within the PS3s (or Po Supersynthem of Fig. 2c; Regione Emilia-Romagna and Eni-Agip, 1998; Regione Lombardia and Eni-Divisione Agip, 2002), whose preservation is favoured by high subsidence rates, reflects Milankovitch-scale (100 kyr) depositional

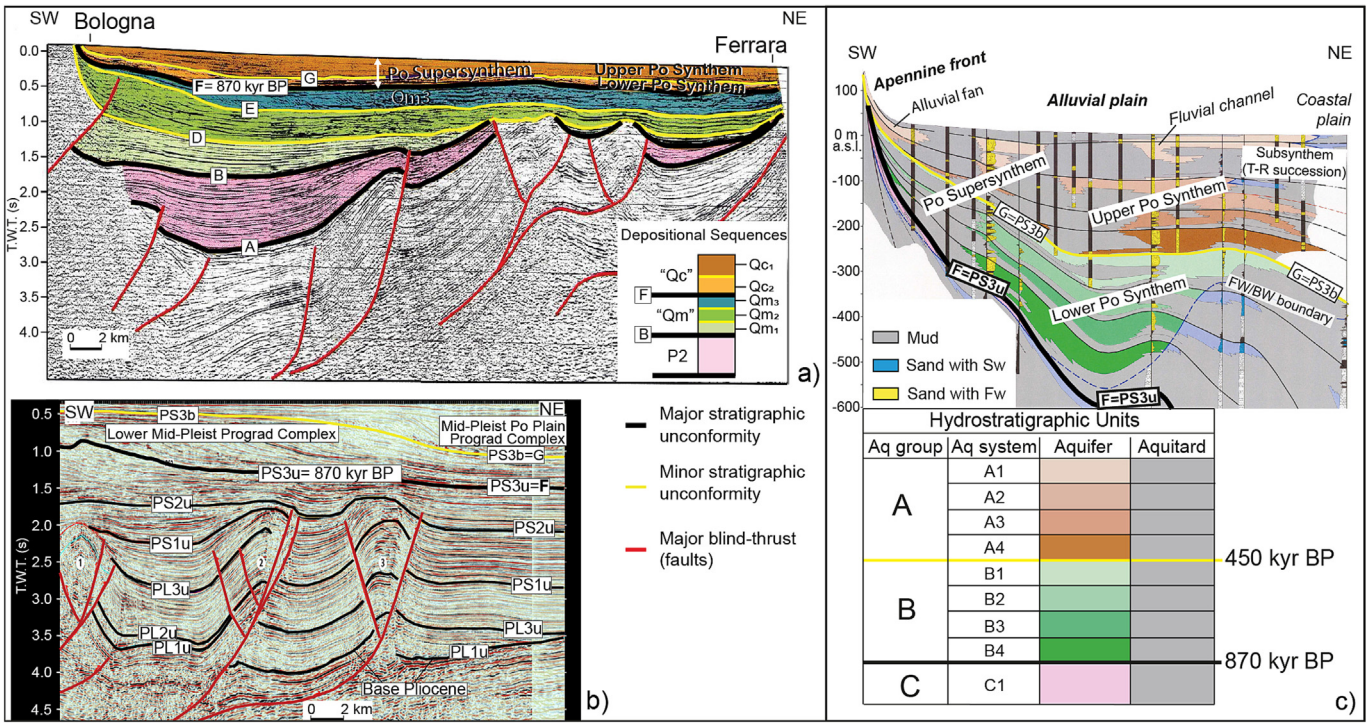

Fig. 2. The stratigraphic framework of the Plio-Quaternary Po-Adriatic Basin. (a) Interpreted seismic profile showing the Pliocene-Quaternary sedimentary infill of the Po Plain onshore sector (modified from Regione Emilia-Romagna and Eni-Agip, 1998; location in Fig. 1). The main depositional sequences (P2, Quaternary marine (Qm), and Quaternary continental (Qc)) and associated tectonic unconformities (A-F surfaces) are highlighted. The Po Supersynthem and its subdivision into lower and upper Po Synthems are also indicated. T.W.T. = two-way travel time. (b) Interpreted seismic profile illustrating the Pliocene-Quaternary succession of the Adriatic offshore sector (modified from Ghielmi et al., 2013; location in Fig. 1). Depositional sequences PL1, PL2, PL3 PS1, PS2 and PS3 follow the reinterpretation of Amadori et al. (2019). Major tectonic unconformities (PL1u-PS3b surfaces) are also displayed. (c) Generalized stratigraphic architecture of the Po Supersynthem (modified from Amorosi and Pavesi, 2010; location in Fig. 1), showing its internal subdivision into Synthems and subsynthems (Transgressive-Regressive – TR – successions). Coarse-grained aquifer bodies are shown in brown and green, and fine-grained aquitards in grey. Abbreviation: Sw = salt water. Fw = fresh water. Aq = Aquifer.

cyclicity in the Po-Adriatic Basin (Bruno et al., 2024). Beneath the coastal plain, partly corresponding to the onshore portion of the study area, PS3s consists of vertically stacked coastal wedges alternating with thick alluvial intervals. These cyclic lithofacies variations, together with changes in fluvial channel stacking patterns within fully alluvial successions at landward position, were linked to glacio-eustatic fluctuations, as indicated by chronological, stratigraphic and palynological data (Amorosi et al., 2004, 2008; Ferranti et al., 2006). Alluvial sediments mainly accumulated during glacial lowstands, whereas coastal wedges and shallow-marine strata were deposited during interglacial sea-level rises and the ensuing coastal progradation (Massari et al., 2004; Fontana et al., 2010; Bruno et al., 2024).

2.5. Hydrogeological setting

From a hydrostratigraphic perspective, coarse-grained fluvial, deltaic, and coastal deposits (gravel and sand) constitute the main aquifer units owing to their petrophysical properties, geometries, and lateral relationships with fine-grained floodplain and shelf sediments, which act as confining units (Regione Emilia-Romagna and Eni-Agip, 1998). Beneath the Po Plain, three major aquifer groups (A, B, and C) have been identified, mainly within the sedimentary fill of the last 870 kyr (Fig. 2c). The top of aquifer group C corresponds to the F/PS3 unconformity. Aquifer groups A and B are separated by the G/PS3b unconformity and are included in the Po Supersynthem/PS3s (Fig. 2c). Aquifer group A (last 450 kyr) comprises four aquifer systems hosted in subsynthems equivalent to transgressive–regressive (T-R) successions. Each succession consists of fine-grained transgressive strata forming aquitards/aquicludes at the base, overlain by fluvial sand bodies that represent the main aquifers, which accumulated mostly during glacial periods (Amorosi and Pavesi, 2010). Within the coastal phreatic aquifer, the water table ranges from 6.1 to 2.4 m a.s.l., with the lowest values in the northern sector and the highest in the study area (Giambastiani et al., 2021). The generally limited and spatially scattered nature of offshore datasets has so far hampered robust evaluation of offshore groundwater extent. Despite necessary assumptions and stratigraphic simplifications, Corradin et al. (2025) recently explored the potential offshore continuation of onshore aquifers of the Venetian-Friulian Plain (first 20 km from the coastline). Their suite of models suggests a high likelihood of onshore-offshore connectivity and underscores the potential of the northern Adriatic shelf for freshwater storage. These results are consistent with earlier OFG assessments in the region (Giustiniani et al., 2022) and with stratigraphic interpretations and recharge mechanisms proposed for potential aquifers beneath the central Adriatic shelf, including active onshore-offshore recharge or recharge during glacial lowstands (Campo et al., 2024). Accordingly, potential OFG bodies within the Adriatic shelf may be sustained by modern meteoric infiltration from Apennine and Alpine rivers in the coastal plains, or by direct rainfall infiltration in areas where fluvial gravels are exposed (e.g. alluvial fans). Alternatively, these aquifers may have been recharged with freshwater during periods of subaerial exposure associated with glacial lowstands. Evidence of low-salinity groundwater in near-coastal settings of the northern Adriatic had been previously inferred from airborne electromagnetic surveys beneath the Venice Lagoon (Teatini et al., 2011). Moreover, the development of bioconcretionary rocky build-ups offshore Venice at about 20 m of water

depth has been attributed to interactions between marine waters and less saline fluids linked to onshore freshwater discharge (Tosi et al., 2017).

3. Methods

The methods used throughout this analysis can be generally described as follows: (1) Dataset, (2) Well log interpretation, (3) Calibration with salinity tests, (4) Sequence stratigraphy-based geological model, (5) Net thickness mapping and volume assessment, (6) Hydrogeological modelling. Fig. 3 illustrates a flowchart summarizing the methodological workflow, outlining the successive steps that guided the analysis and led to the principal findings of this study.

3.1. Dataset

This study is entirely based on the reinterpretation of legacy subsurface data acquired over the past 65 years for hydrocarbon exploration (Azienda Generale Italiana Petroli Mineraria, 1959), onshore groundwater investigations (Regione Emilia-Romagna and Eni-Agip, 1998; Regione Lombardia and Eni-Divisione Agip, 2002), and geological mapping activities across the Po-Adriatic Basin (Fig. 1). These data are now publicly available through the ViDEPI Project (https://www.videpi.com/videpi/pozzi/consultabili.asp) and the Geological Survey of Regione Emilia-Romagna (https://ambiente.regione.emilia-romagna.it/it/geologia/servizi-e-strumenti/cartografie-webgis/prove-geognostiche-e-geotecniche-1). A total of 28 composite well logs (11 onshore, 17 offshore) from the ViDEPI database and 28 onshore water wells were re-evaluated in terms of lithofacies and formation water type, focusing on the distinction between high-permeability (aquifer) and low-permeability (aquitard/aquiclude) units, and correlated along four onshore-offshore transects (traces in Fig. 1). The composite logs, mostly produced by ENI and following American Petroleum Institute (API) standards (Fig. 4), include lithological descriptions (from cuttings and Spontaneous Potential – SP – logs), formation names and ages, depth (in metres), geophysical logs (Spontaneous Potential and resistivity), and indications of fluid content and type (fresh water, brackish water, salt water). Additional information includes depositional environments, biostratigraphy, drilling mud types, and locally chemical analyses (TDS in mg/L) from selected intervals (Fig. 5).

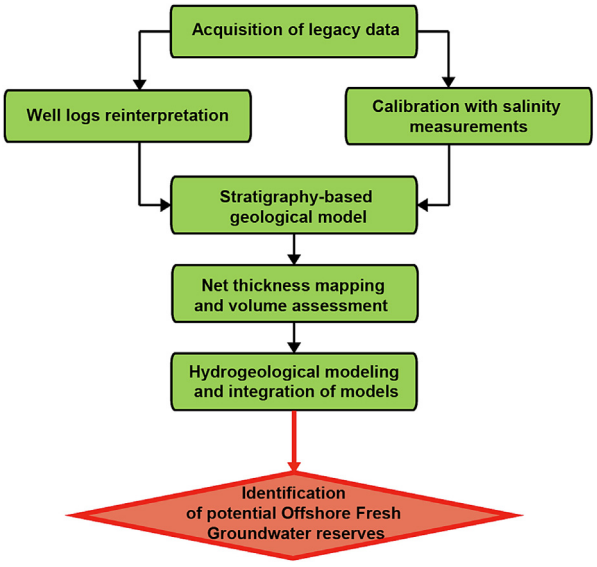

Fig. 3. Methodological flowchart. Overview of the workflow adopted in this study, illustrating the sequence steps from data acquisition and processing to hydrostratigraphic reconstruction, volumetric assessment and hydrogeological modelling for the identification of offshore fresh groundwater reserves.

3.2. Well log interpretation

Petrophysical analysis of well logs enables the estimation of key reservoir properties, such as porosity and water saturation (Rider and Kennedy, 2011). This study primarily relies on Spontaneous Potential (SP) and resistivity logs, to assess formation water salinity and lithological characteristics, as shown in Fig. 4.

SP logs are measured in millivolts (mV), with deflections of the profiles interpreted relative to a defined shale baseline (Fig. 4). The maximum SP deflection should represent a permeable (i.e., gravel to sand) water-bearing formation with no shale (Fig. 4). The mud used during drilling, e.g. the "mud filtrate", commonly invades the formation adjacent to the borehole and replaces connate fluids, influencing the log response. The salinity contrast between the formation water and the mud filtrate largely controls the direction of SP deflections (Rider and Kennedy, 2011). Leftward SP shifts generally suggest more saline formation water (Fig. 4a) or, alternatively, a mud filtrate that is fresher than the in-situ fluids, as shown in Fig. 4b at 330 m depth. Conversely, rightward deflections typically reflect fresh water (or fresher formation water), as observed at ca. 260–270 m and 310–325 m depth in Fig. 4b. To properly account for these effects, the workflow integrated detailed records of the drilling-mud types used during the acquisition of each of the 28 wells, as reported in the ViDEPI log descriptions. In sand-shale sequences, like those from the Po-Adriatic Basin, SP logs can be used for qualitative lithofacies recognition as the SP shape is related to the shale content, with full SP for clean sandy strata and diminishing SP over shaly intervals (Fig. 4). SP curves may be useful for identifying coarsening- or fining-upward sequences typical of deltaic and fluvial deposits (Fig. 4; after Hawkins, 1972). SP logs are also useful for stratigraphic correlation in regions with variable salinity (Rider and Kennedy, 2011).

Resistivity logs complement SP analysis by quantifying a formation's capacity to conduct electrical current flow, primarily governed by pore-water content and salinity. Saline water (SW) formations generally exhibit low resistivity (Fig. 4a), whereas freshwater (FW)-bearing formations show high resistivity (Fig. 4b). Clay minerals may locally reduce resistivity due to their conductive properties (Rider and Kennedy, 2011). Because mud invasion typically affects the first 2 m around the borehole, resistivity logging tools are equipped with shallow and deep investigation tools. Shallow measurements record the resistivity of the "invaded zone", whereas deep-reading tools (depth of investigation > 2 m, up to 5 m) detect the resistivity of the "uninvaded", or "virgin" formation (Schlumberger, 1989). The contrast between shallow and deep resistivity is diagnostic of different fluid types, including SW and FW formation water (Rider and Kennedy, 2011; Fig. 4). In SW-bearing formations, SP deflects to the left and both shallow and deep resistivity values are low, with minimal difference (Fig. 4a). In FW-bearing formations, SP deflects to the right and deep resistivity exceeds shallow resistivity (Fig. 4b). Resistivity is measured in ohm·m (Ω·m). All well logs analysed in this study were acquired with comparable logging suites, including both deep- and shallow-reading resistivity tools, which provided key information for the reinterpretation and the identification of the original formation water, avoiding the mud effect.

3.3. Calibration with salinity measurements

Spontaneous Potential (SP) and resistivity logs were calibrated against formation-water salinity measurements (expressed as NaCl

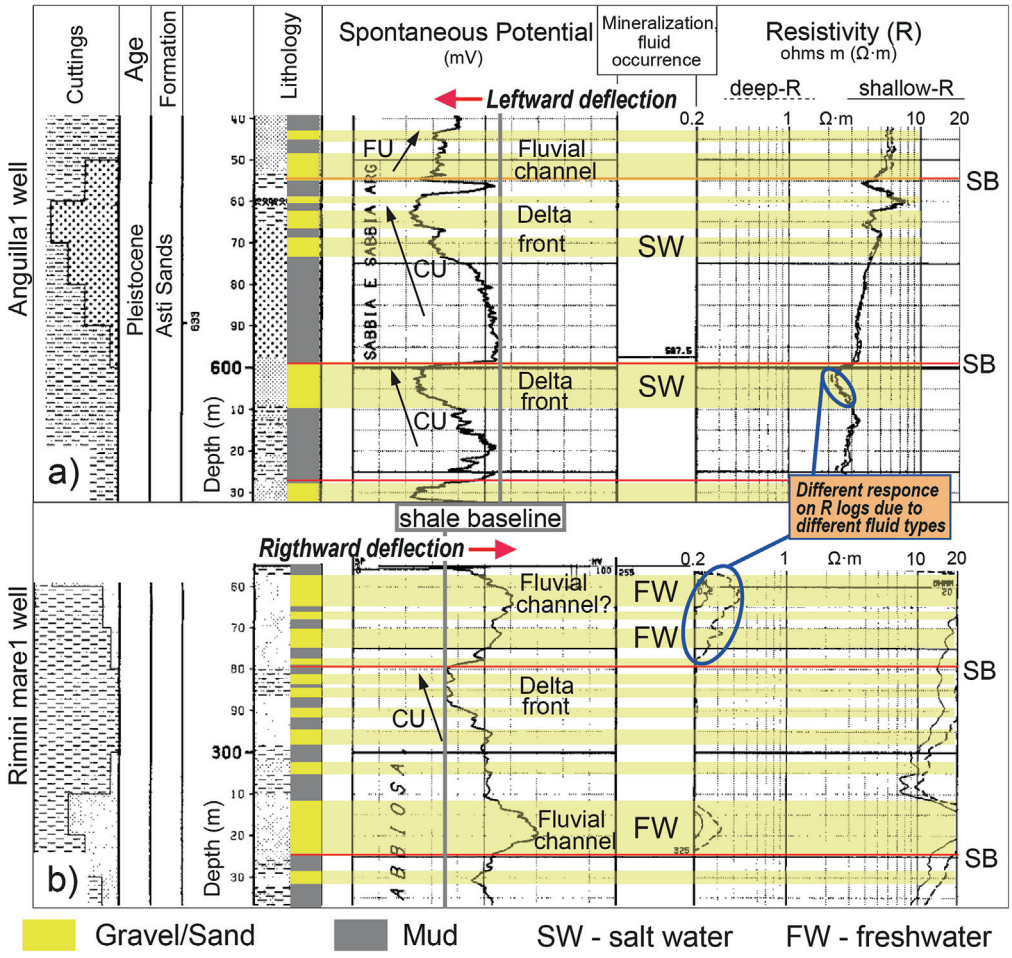

Fig. 4. Reinterpreted ViDEPI well logs. Reinterpretation of representative ViDEPI well logs (well locations in Fig. 1), showing lithology, shale baseline (light-blue line), fourth-order sequence boundary (SB), and grain size trends (coarsening-upwards, CU; fining-upward, FU). (a) Leftward Spontaneous Potential (SP) deflection: mud filtrate salinity lower than formation water, indicating more saline formation water. (b) Rightward SP deflection: formation water less saline than mud filtrate, indicating freshwater-bearing intervals. "Fluvial ch?" marks tentatively interpreted as fluvial-channel deposits. R = resistivity.

concentration – Fig. 5) derived from chemical analyses of samples collected from selected stratigraphic intervals of four wells (Greta, Mesesano2, Medesano6 and Tollara1) recovered from the Po-Adriatic Basin and available from the ViDEPI dataset (Fig. 1).

Although located outside the study area, these well logs intersect lithologies and stratigraphic intervals that are equivalent (Medesano2-6, Tollara1) or broadly comparable (Greta) to those examined in this study. Fig. 5 shows the one-to-one calibration between SP/resistivity log signatures and measured formation-water salinities. As described above, both SP and resistivity exhibit salinity-dependent variations (Fig. 4), and the combined interpretation of these parameters alongside salinity data enhances calibration robustness. For each interval, SP deflections, shallow/deep resistivity responses, and NaCl concentrations were jointly evaluated to define salinity-resistivity classes representative of the groundwater types hosted within the investigated succession. A NaCl concentration of 29,470 mg/L was measured in an interval characterized by minor, high-frequency SP deflections, with shallow and deep resistivity values ranging between 2–4 Ω·m, (Fig. 5a). A second interval of the same well and showing similar SP behaviour but slightly higher resistivity values (4–5 Ω·m), corresponded to a salinity of 13,096 mg/L (Fig. 5a). Two permeable units yielded salinities of 3500 and 3000 mg/L and were associated with leftward SP deflections and deep resistivities of 6 and 9 Ω·m, respectively (>5 Ω·m; Fig. 5b). The lowest measured salinity (50 mg/L) was recorded in a permeable interval with generally leftward SP deflections and the highest deep resistivities (24–30 Ω·m; Fig. 5c).

To validate the calibration and the resulting salinity-resistivity ranges, these measured values were compared with existing salinity-resistivity and sediment-type relationships (Nowroozi et al., 1999). This comparison enabled refinement of the calibration and allowed identification of four main pore-water formation classes (seawater, salt water, brackish water and fresh water), as summarized in Table 1. A conservative threshold of 15 Ω·m was adopted to distinguish fresh (>15 Ω·m) from brackish (<15 Ω·m) groundwater. This threshold is more conservative than the classification proposed by Regione Emilia-Romagna and Eni-Agip (1998), who considered units with resistivity >10 Ω·m as freshwater-bearing. The threshold between brackish and saline water was set at 5 Ω·m, whereas resistivity values <2 Ω·m indicate seawater-level salinities (Table 1; after Nowroozi et al., 1999; Voutchkov, 2018).

3.4. Sequence stratigraphy-based geological model

To reconstruct the architecture and distribution of aquifers and aquitards/aquicludes, the most recent sequence stratigraphic concepts have been applied (Neal et al., 2016; Pellegrini et al., 2017a). Although sequence boundaries (SBs) play a central role in the clas-

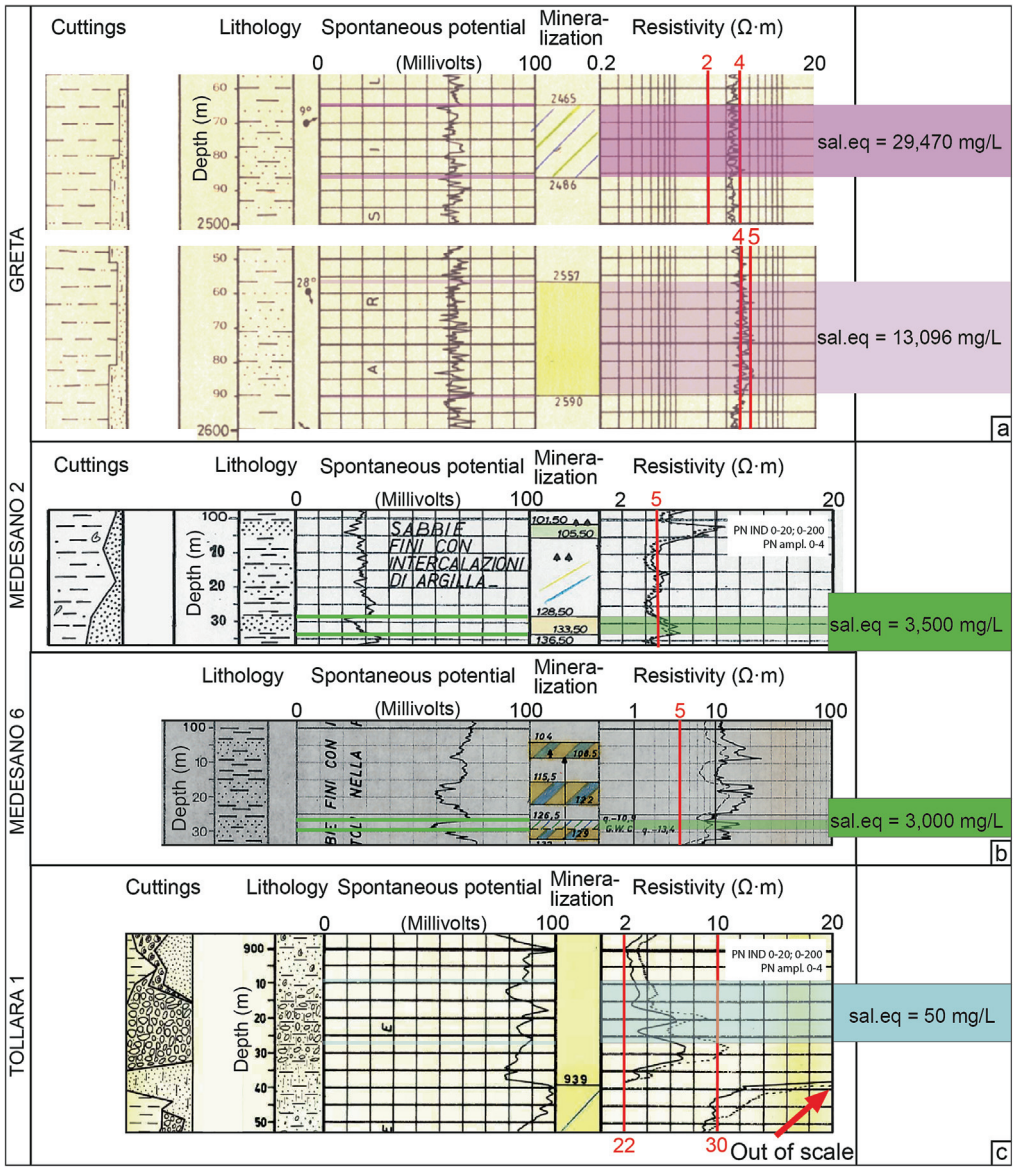

Fig. 5. Calibration of spontaneous potential (SP) and resistivity curves with formation water salinity. Salinity analyses were obtained from the ViDEPI dataset for the wells Tollara1, Medesano2, Medesano6 and Greta (location in Fig. 1). (a) Calibration in the Greta well. Two salinity analyses are available for two stratigraphic intervals: 29,470 mg L^{-1} corresponds to resistivity values of 2–4 Ω·m, and 13,096 mg L^{-1} corresponds to 4–5 Ω·m. (b) Calibration in the Medesano2 and Medesano6 wells. In Medesano2, a salinity content of 3500 mg L^{-1} corresponds to resistivity values >5 Ω·m, while in Medesano6, 3000 mg L^{-1} corresponds to 5–11 Ω·m. (c) Calibration in the Tollara1 well. A salinity of 50 mg L^{-1} corresponds to resistivity values of 22–30 Ω·m (>20 Ω·m is considered out of scale). Sal. eq = salinity equivalent.

Table 1
Resistivity of water and sediments. Data modified after Nowroozi et al. (1999) and Voutchkov (2018).

Resistivity (Ω·m)	Sediments	Interpretation
<2.0	Very porous sand, or saturated clay	Seawater; TDS > 30,000 mg L^{-1}
2.0–4.0	Porous sand, or saturated clay	Very saline water; 20,000 < TDS < 30,000 mg L^{-1}
4.0–5.0	Sandy saturated, or sandy clay	Saline water; 10,000 < TDS < 20,000 mg L^{-1}
5.0–9.0	Sandy saturated, or sandy clay	Salty brackish water; 3000 < TDS < 10,000 mg L^{-1}
9.0–15.0	Sandy clay, sandy gravel	Brackish water; 1500 < TDS < 3000 mg L^{-1}
>15.0–30.0	Sand, gravel, some clay	Poor quality fresh water; 100 < TDS < 1500 mg L^{-1}
>30.0	Sand, gravel, minor clay	Good quality fresh water; TDS < 100 mg L^{-1}

sical approach (Mitchum et al., 1977; Vail et al., 1977), regional groundwater studies in the Po Plain typically used the transgressive surface (TS), also termed the "*maximum regression surface*" (Catuneanu et al., 2009), as the main reference surface for aquifer mapping. This choice was largely pragmatic, as TSs were generally easier to recognize and interpret than other surfaces within the Po Plain basin fill (Amorosi and Colalongo, 2005; Amorosi and Pavesi, 2010). However, the "TS-like" mapping based solely on formation tops may obscure lateral trends and groundwater-flow connectivity (Campo et al., 2020). Conversely, SB-based mapping can better delineate aquifer units and refine predictions of their spatial distribution, particularly in linking onshore fluvial and offshore deltaic systems deposited during glacio-eustatic lowstands (Campo et al., 2024). Stratigraphic reconstruction also incorporated sea-level fluctuations, sedimentation rates, tectonic activity, and subsidence. Using well log data, supported by seismic profiles and information available for the offshore sector (Ghielmi et al., 2010, 2013;

Amadori et al., 2019), the geometries, thicknesses, spatial distribution, and stacking patterns of aquifers and aquitards/aquicludes were reconstructed along coastal-to-shelf profiles (Fig. 1). These data enabled the basin-wide correlation of the three major (*third-order*) unconformities (PS2u, PS3u and PS3ub) marking the major shifts in depositional systems and gross sediment architecture. These unconformities were identified in well logs based on major changes in the type and gross distribution of the depositional systems. To evaluate glacio-eustatic controls on aquifer stratigraphy, offshore well-logs were integrated with the ultra-high-resolution onshore stratigraphic record (Amorosi et al., 2004). Beneath the coastal plain, the SB coincides with the subaerial unconformity formed during the MIS 5e/5d transition, corresponding to the last Interglacial/glacial sea-level fall (Amorosi et al., 1999). The offshore equivalents of these unconformities consist of erosional surfaces passing seaward into correlative conformities (Ridente et al., 2009). SBs were therefore traced offshore to subdivide the sedimentary succession into *fourth-order* Milankovitch-scale sequences (~100 kyr).

3.5. Net thickness mapping and volume assessment

Based on the available data coverage (Fig. 1) and on the stratigraphic cross sections defining the hydrostratigraphic framework of the study area, net thickness mapping and volumetric analysis of the aquifer units were performed using Petrel software (Schlumberger). Thickness maps were realized to illustrate the overall thickness and areal extent of low-salinity groundwater-bearing aquifers beneath the Adriatic shelf. All wells located within the study area (Fig. 1) were analyzed. Additional wells located outside the four reference cross sections were incorporated by constructing an expanded set of stratigraphic transects perpendicular to the main reference profiles. This approach ensured consistent three-dimensional correlations across the study area and improved the definition of aquifer geometries and lateral facies relationships. These data were further used to validate and refine the mapped geometries, enhancing the robustness of the reconstructed hydrostratigraphic model. For map construction, the convergent interpolation method available in Petrel was selected as the most suitable approach to interpolate net thickness values, owing to its high spatial reliability and iterative control-point-oriented refinement (Geach et al., 2014). Grid geometry and cell size were automatically defined from the spatial distribution of the input wells and the boundary polygon of the study area, resulting in a *x-y* grid increment of 50 m. A Taylor series projection was applied as the base gridder, and the Briggs biharmonic (minimum curvature) algorithm (Briggs, 1974) was used to generate smooth surfaces. Final thickness maps were slightly refined through minor manual editing to fully incorporate hydrostratigraphic interpretations and geometrical trends from the cross sections.

Decompacted sediment volumes were estimated for the last 870 kyr PS3 sequence (PS3s) stratigraphic succession, with main focus on the volumetric quantification of fresh and brackish water stored in the lower- and upper-PS3s. This stratigraphic subdivision is important to shed light on the different processes controlling the groundwater emplacement, as it reflects a different tectono-sedimentary evolution of the study area: the lower-PS3 (870–450 kyr BP) accumulated during a phase of active tectonic uplift, whereas the upper-PS3 was deposited under tectonic quiescence during the last 450 kyr.

Aquifers volumes have been assessed by using the volume calculation tool available in the software Petrel. Porosity values, measured in the Casaglia well (Fig. 1) at different stratigraphic intervals of the aquifer groups A and B (Regione Emilia-Romagna and Eni-Agip, 1998), were used to convert aquifer volumes into estimates of stored groundwater. Aquifer groups A and B correspond to the upper and lower interval of the PS3 sequence, respectively (Fig. 2). A total of 13 porosity measurements were available for Group A and 14 for Group B, yielding mean porosity values of 38.2% and 37.6%. These values are consistent with independent porosity estimates derived from geophysical logs (Fig. 1), which indicate similar high porosities (33%–45%) for the same aquifer groups (Regione Emilia-Romagna and Eni-Agip, 1998). Such elevated porosity values reflect both the predominantly coarse-grained lithology of fluvio-deltaic sediment bodies forming these aquifers and, potentially, post-depositional dissolution (Regione Emilia-Romagna and Eni-Agip, 1998). Given the range of porosity values documented for the PS3 sequence, a quantitative sensitivity analysis was carried out to evaluate how this variability may influence volumetric estimates of freshwater and brackish water aquifers. Three porosity scenarios were examined, reflecting the range documented from core measurements and geophysical logs: (1) a conservative lower-end value of 33%; (2) a central representative value of 38%; (3) an upper-bound value of 45%. For each stratigraphic interval (lower-, upper- and total PS3s), pore water volumes were recalculated by multiplying the bulk sediment volume by the selected porosity value. Due to the lack of data for the uppermost stratigraphic interval, thickness and volumes are underestimated for the upper-PS3s.

3.6. Hydrogeological modeling

The hydrogeological modelling was performed by programming in Matlab™, the analytical model developed by Oude Essink (2000) and represented in Eqs. (1)–(4), which is appropriate for a confined coastal aquifer and accounts for density-controlled flow. The model relies on the following assumptions: (i) the whole aquifer package is confined at the top and bottom from impermeable units, and (ii) the continuity, Darcy, and Ghyben-Herzerg laws are satisfied (Oude Essink, 2000), which appears to be a very reasonable assumption based on the high-resolution stratigraphic framework presented below (Fig. 6) and the mostly low-velocity parallel flow in the aquifer package. The formulation of the analytical solution used for determining the length of a saltwater wedge L is the following:

$$H = \sqrt{\frac{-2q_0 x}{K\alpha}} \tag{1}$$

$$h = \alpha(H + A) \tag{2}$$

$$q = q_0 \tag{3}$$

$$L = \frac{kD^2\alpha}{2q_0} \tag{4}$$

where, H is the depth of the freshwater-saltwater interface from the bottom of the confining unit (L); x is the distance from the tip point of the freshwater unit (L); K is the hydraulic conductivity of the aquifer (L/T) that we compute from arithmetic mean for parallel flow (Fetter, 2014) using the sand/mud ratio, and the K for the sandy and muddy layers; q_0 is the horizontal flow rate seaward (recharge) (L/T); α is the Ghyben-Herzerg density contrast constant ($-$); D is the thickness of the saturated aquifer (L); A is the depth of the top of the aquifer from sea level (L); L is the length of the saltwater wedge (L).

Based on several measurements carried out in different locations of the Adriatic sandy coastal aquifers (Ripa and Pitoni, 2001; Antonellini et al., 2008), the hydraulic conductivity (K) varies in the range 0.1–1 m/d. To reconstruct the positions of the interface between fresh water and salt water, the following parameters have shown the best fit to the well data:

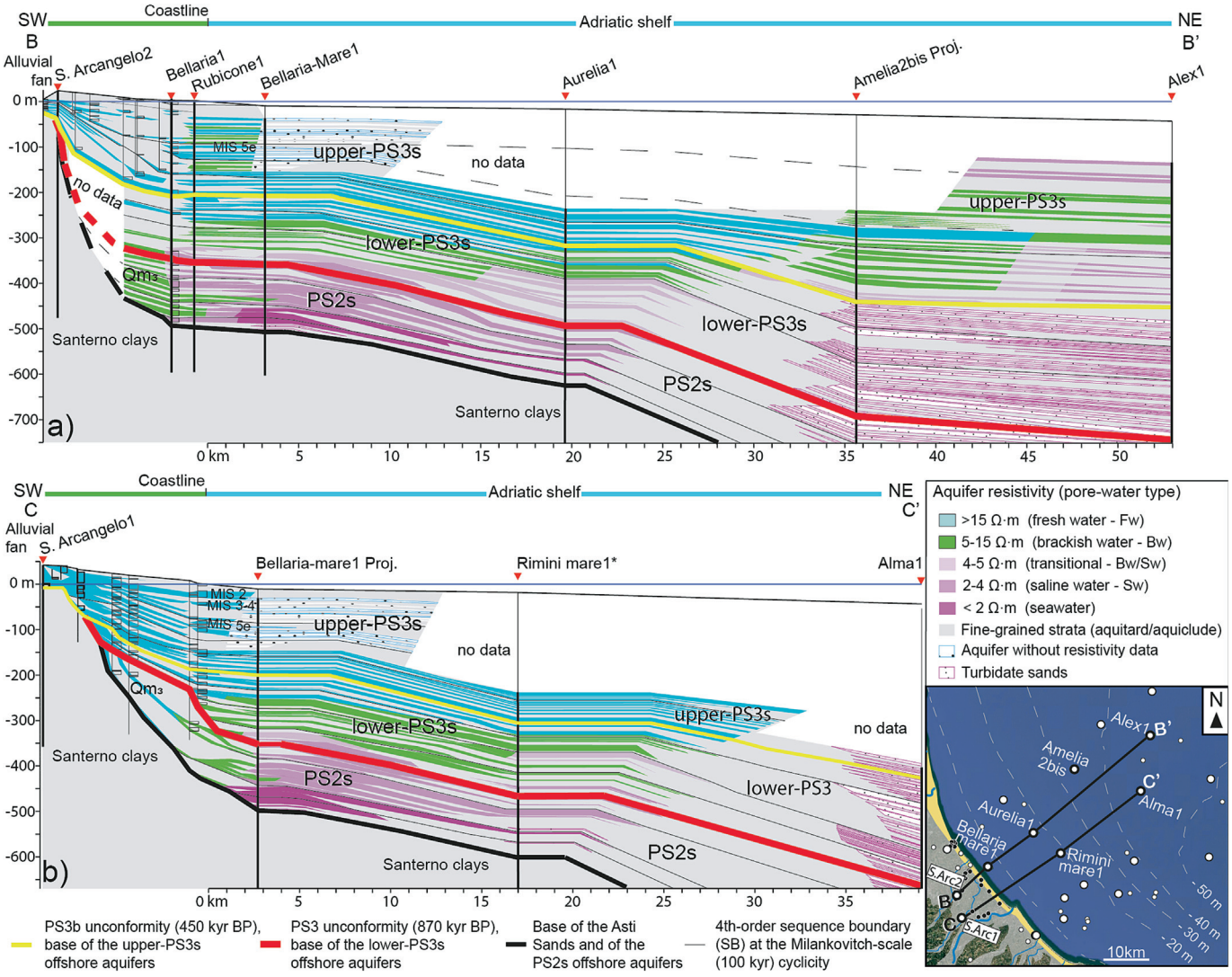

Fig. 6. Reference hydrostratigraphic transects. Onshore-offshore correlation of well logs (red triangles) and water wells (coastal sector only; Regione Emilia-Romagna Geological Survey database) along the reference transects (the location of the transects is shown in the lower-right map). Different stratigraphic intervals (PS2s, lower- and upper-PS3s) and main basal unconformities are indicated. Aquifers correspond to coarse-grained bodies in different colours, whereas aquitards and aquicludes are shown in grey. MIS_Marine Isotope Stage. Qm_3: Quaternary marine cycle 3. (a) Hydrostratigraphic setting along transect B-B' (location in Fig. 1). (b) Hydrostratigraphic setting along transect C-C' (location in Fig. 1). Proj. = projected well. *Isola delle Rose site.

- K for sandy deposits is 0.1 m/d;
- shale gouge ratio is 0.6 (this has been derived by the stratigraphic logs and is used to compute the average hy draulic conductivity of the aquifer package);
- shale hydraulic conductivity is $1x10^{-6}$ m/d; D is 500 m;
- and the horizontal flow rate q_0 is 6.85×10^{-4} m/d, equivalent to a 250 mm/year recharge.

By assuming a Ghyben-Herzberg constant of 28, which is typical for the salinity of the Adriatic Sea (Giambastiani et al., 2007), and by obtaining the L, A, D parameters from the hydrostratigraphic transects of Fig. 6, we can invert to obtain the recharge (q_0). If the offshore aquifers are actively recharged by meteoric precipitation, the computed q_0 must be like the q_0 estimated for the coastal aquifer in the area (Antonellini et al., 2015). At present, the offshore aquifers are recharged by rainfall infiltration in proximity of the Apennine alluvial fans. This process likely also occurred during the lowstand periods of the Pleistocene.

4. Results

The coastal-to-shelf stratigraphic correlation allowed the reconstruction of the along-dip stratal architecture Po-Adriatic succession dated to Lower Pleistocene-Holocene (Figs. 6 and 7). The high-resolution geometrical representation of the coarse-grained sedimentary bodies (i.e., aquifers), their lateral extent and vertical relationship with fine-grained strata (i.e., aquitards/aquicludes), together with calibrated resistivity values provided reliable information about the salinity of the pore water (Figs. 6 and 7). Because of their seaward extent, quality, quantity of data, and the information provided, cross sections B-B' (Fig. 6a) and C-C' (Fig. 6b) were first described as the reference hydrostratigraphic panels. On the other hand, although cross sections A-A' and D-D' are less complete or may document similar characteristics in terms of aquifers' architecture as those shown in Fig. 6, they are representative of the northernmost (Fig. 7a) and southernmost (Fig. 7b) sectors of the study area, respectively. To avoid redundant descriptions and concepts, only the main differences between the reference and the

additional panels have been highlighted below. Furthermore, to provide an overview of the spatial distribution of the aquifer systems and reveal their accumulation through the main geological phases, net thickness maps have been produced across the study area. As saline groundwater cannot be considered a useful resource, only freshwater (Fig. 8) and brackish water (Fig. 9) aquifer units have been mapped. Finally, to assess resource sustainability and recharge potential of aquifer systems, a hydrogeological model (Fig. 10) has been developed.

4.1. Onshore-offshore hydro-stratigraphy

Above the marine clays of the "Santerno Formation", the lowermost main unconformity marks the base of the "Asti Sands Formation" and the onset of Lower Pleistocene (Zecchin et al., 2017) deposition of increasingly coarser-grained shelf-to-coastal and deltaic strata of the PS2 sequence (PS2s, Fig. 6). The combination of their vertical stacking and the gradual NE-directed shift of depositional environments suggests an overall progradational trend of the PS2s. Coastal and deltaic gravel and sand bodies laterally transition to shelf muds at distal locations, whereas deep-marine turbidites are disconnected (Fig. 6). Up-dip, coastal and deltaic deposits are laterally connected with progressively more inclined gravel bodies with tabular geometry of the Qm_3 cycle (Fig. 6). In the southern area (Fig. 6b), Qm_3 deposits are directly connected with the alluvial fan gravels of the overlaying PS3 sequence (PS3s) through the erosional unconformity PS3u. The latter is dated to the latest major uplift of the Apennines (e.g., 870 kyr BP) and corresponds to the PS2s/PS3s boundary (Fig. 6b). The Lower-to-Middle Pleistocene PS2s displays a general but gradual decrease of resistivity values from onshore to offshore sectors (Fig. 6), with high resistivities in the band of fresh pore-water (> 15 Ω·m) only beneath the modern coast at southern locations (Fig. 6b). Here, 3 km inland from the coastline and above the deepest coarse-grained bodies characterized by medium (5–15 Ω·m) to low (<2 Ω·m) resistivity, Qm_3 gravels and sands show high resistivities, suggesting fresh pore-water content despite their marine origin. Resistivity progressively decreases down-dip to values characteristic of brackish and saline (2–4 Ω·m) pore water. On the contrary, the PS2s do not contain any freshwater bodies in the northern sec-

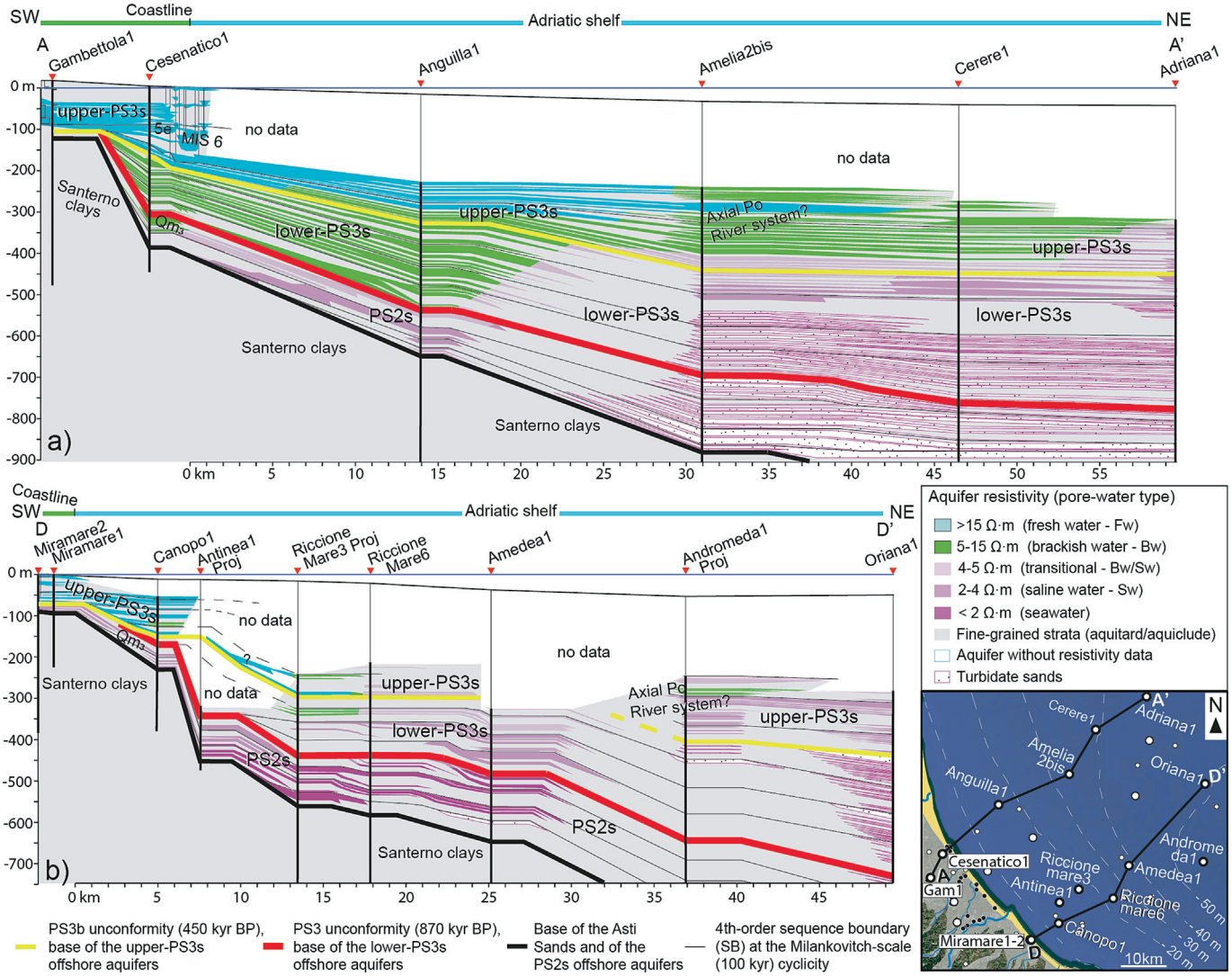

Fig. 7. North and south hydrostratigraphic transects. Hydrostratigraphic transects A-A' and D-D' (the location of the transects is shown in the lower-right map) showing onshore-offshore correlation of well logs (red triangle) and water wells (coastal sector only; Regione Emilia-Romagna Geological Survey database). Different stratigraphic intervals (PS2s, lower- and upper-PS3s) and main basal unconformities are indicated. Aquifers correspond to coarse-grained bodies in different colours, whereas the aquitards and aquicludes are shown in grey. MIS = Marine Isotope Stage. Qm_3 = Quaternary marine cycle. (a) Hydrostratigraphic setting along transect A-A' (location in Fig. 1). (b) Hydrostratigraphic setting along transect D-D' (location in Fig. 1). Ap = Apennine system. Po= Po system. Proj. = projected well.

tor, where the Qm_3 coarse-grained bodies are disconnected from the overlaying, higher-resistivity alluvial fans (Fig. 6a). At offshore locations, the PS2s aquifers display low resistivities typical of saline water (Fig. 6).

Above the PS3u, the PS3s records an even stronger progradational trend (Fig. 6). The identification of the PS3b unconformity (PS3ub) allowed the internal subdivision of the PS3s into lower- and upper-PS3 units (Fig. 6). This erosional unconformity mimics PS3u at the basin margin, where it forms an equivalent angular unconformity within the amalgamated alluvial-fan gravels of the lower- and upper-PS3s (Fig. 6b). In wells, beneath the Adriatic shelf, the PS3b marks the onset of an additional NE-directed shift of the Apennine fluvio-deltaic systems, with the shelf-edge limit further migrating basinward, around 35 km from the modern coastline (Amelia2bis well, Fig. 6a). The lower-PS3 interval, within the first 15 km offshore (320–250 m depth), is mostly dominated by brackish water aquifers, representing the mixing zone between freshwater and saline water (Fig. 6). The mixing zone extends additional 10 km offshore between Bellaria-Mare1 and Aurelia1 wells (Fig. 6a), and Bellaria-Mare1 and Rimini-Mare1 wells (Fig. 6b), respectively. In the lower-PS3s, freshwater aquifers are up to 8 m-thick and show lateral continuity through the coastal-to-the shelf sector reaching their maximum offshore extent nearby the wells Aurelia1 and Rimini-Mare1, between 350 and 300 m depth (Fig. 6).

The upper-PS3s is mostly dominated by alternating, laterally continuous muddy strata and coarse-grained deposits (Fig. 6). The latter are widespread along the transects and consist of generally tabular, up to 10 m thick, fluvial sand bodies laterally transitioning to amalgamated alluvial fan gravels and deltaic-to-coastal sediments at proximal and distal sectors, respectively (Fig. 6). At distal locations (Amelia2bis well, Fig. 6a), deltaic sand bodies are up to 20 m thick. Overall, the offshore extent of sand bodies exceeds 35 km, about 15 km more than equivalent deposits from the lower-PS3s (Fig. 6a).

The upper-PS3s show a generalized increase in resistivity, and vertically-confined freshwater aquifers become a frequent occurrence (Fig. 6), especially in the southern sector. These systems generally represent the offshore continuity of coastal aquifers beneath the Adriatic shelf. They store freshwater within the first 35 km offshore (Fig. 6a) and brackish water further downdip (>50 km, Fig. 6a).

4.2. Northern and southern hydro-stratigraphic panels

The two additional hydrostratigraphic transects shown in Fig. 7 document corresponding unconformities, sequences, deposits, and progradational trends as those of Fig. 6. Similarly, the resistivity patterns, as well as the general aquifer geometries, their lateral extent and vertical relationships with aquitards/aquicludes resemble those described above.

Unlike the reference panels, PS2s offshore aquifers contain only saline water (Fig. 7). On the other hand, brackish water occurs in the PS2 interval but just below the modern coastline at the northernmost locations (Fig. 7a). In this sector, no fresh water was identified within the lower-PS3 that is entirely dominated by brackish water, considering the first 15 km offshore and down to about 550 m below sea level (b.s.l. – Fig. 7a). These aquifers seem disconnected from the alluvial fan at proximal locations, unlike their equivalents displayed in Fig. 6. In the opposite sectors of the study area, freshwater bodies were only found above about 300 m b.s.l., and within the upper-PS3s (Fig. 7b). However, the maximum offshore extent of freshwater reserves is about 31 km and 13.5 km for the northern and the southern sectors, respectively (Fig. 7). Both transects show that the aquifers of the upper-PS3s are likely connected to their onshore equivalents and alluvial fans. A major and comparable offshore extent in the northern area is also documented for the brackish aquifers (Fig. 7a). The latter were detected up to 46 km from the modern shoreline to the north (Fig. 7a). Southward, brackish water characterizes only a thin interval (mixing zone) between 300 and 270 m b.s.l., near the Andromeda1 well (Fig. 7b). Despite the lack of data, this isolated brackish aquifer unit (Riccione-Mare3 well, Fig. 7b) seems disconnected from its landward (i.e., Apennines) equivalent. Stratigraphic correlation and additional seismic data (Fig. 2b; after Ghielmi et al., 2013) suggest that this aquifer could be part of the axial Po River system merging with the Apennine system in this part of the basin (Fig. 7).

4.3. Net thickness of freshwater aquifers and pore water volumes assessment

Fig. 8a represents the total net thickness of the aquifers containing fresh water (FW) within the PS3s, as well as their lateral extent beneath the modern shelf. To better constrain the tectonic and stratigraphic control on the offshore FW emplacement and distribution, the maps of Fig. 8b and 8c display the total net thickness of FW aquifers within the lower- (870–450 kyr BP) and the upper-PS3 (last 450 kyr) units, respectively. For each stratigraphic interval, the FW volume was quantified under three porosity scenarios (33%, 38%, and 45%), selected to represent the observed variability within the PS3s deposits (Table 2). Because of the lack of data shown in Figs. 6 and 7, thickness and volumes are underestimated for the upper-PS3s.

The largest thickness values of the aquifer units are recorded below the modern coastal plain and gradually decrease toward the offshore sector within the first 40 km from the coastline (Fig. 8a). North and west of Rimini, in coincidence with the Apennine margin, two main depocenters exceed 75 m and 100 m in thickness (Fig. 8a). The thickest depocenter corresponds to the alluvial fan of the Marecchia River (Severi et al., 2014), whereas the second one is located below the modern Rubicon River mouth (Fig. 8a) that probably acted as the major sediment entry points. It is likely that also the Savio River nourished this depocenter by supplying a considerable amount of coarse-grained material at different times when it flowed to the east (Fig. 8a). Within the first 15–20 km from the coastline, these two depocenters coalesce and are slightly elongated in a NE direction (Fig. 8a), in agreement with the progradational trend of PS3s. Their semi-circular shape (Fig. 8) is consistent with fluvio-deltaic depositional systems dominated by fluvial processes (Bhattacharya, 2006). In this sector of the shelf, mean aquifer thickness ranges between from 75 m to 50 m (Fig. 8a), and progressively decreases to 25 m downdip where the aquifer bodies generally thin out and are in lateral transition with aquitards, with FW replaced by brackish water (Fig. 6).

This general thickness distribution and lateral extent of FW aquifers is also displayed in Fig. 8b and 8c. However, the FW aquifers of the lower-PS3s show considerably lower thickness (maximum about 25 m) and smaller offshore extent (maximum 20 km from the coastline, Fig. 8b) than the upper-PS3s FW aquifers (Fig. 8c). The latter exceed 75 m in total thickness below the modern Marecchia River alluvial fan and 50 m near the second depocenter to the north (Fig. 8c). Other than these two Apennine depocenters elongated to the NE, a third depocenter, up to 25 m thick and located in the northernmost offshore location, shows a SE direction (Fig. 8c). This depocenter corresponds to the stratigraphic interval characterized by the up to 20 m-thick aquifer bodies between Amelia2bis and Alex1 wells (Fig. 7a). Thickness and depocenter orientation suggest the paleo-Po Delta system as the sediment entry point. This interpretation is supported by seismic data showing the south-eastward progradation of the Po-Plain Complex during the last 450 kyr, and its gradual merging with the Apennine systems in this area (Fig. 2b). It is likely that the paleo-Po Delta system prograded from the north down to this sec-

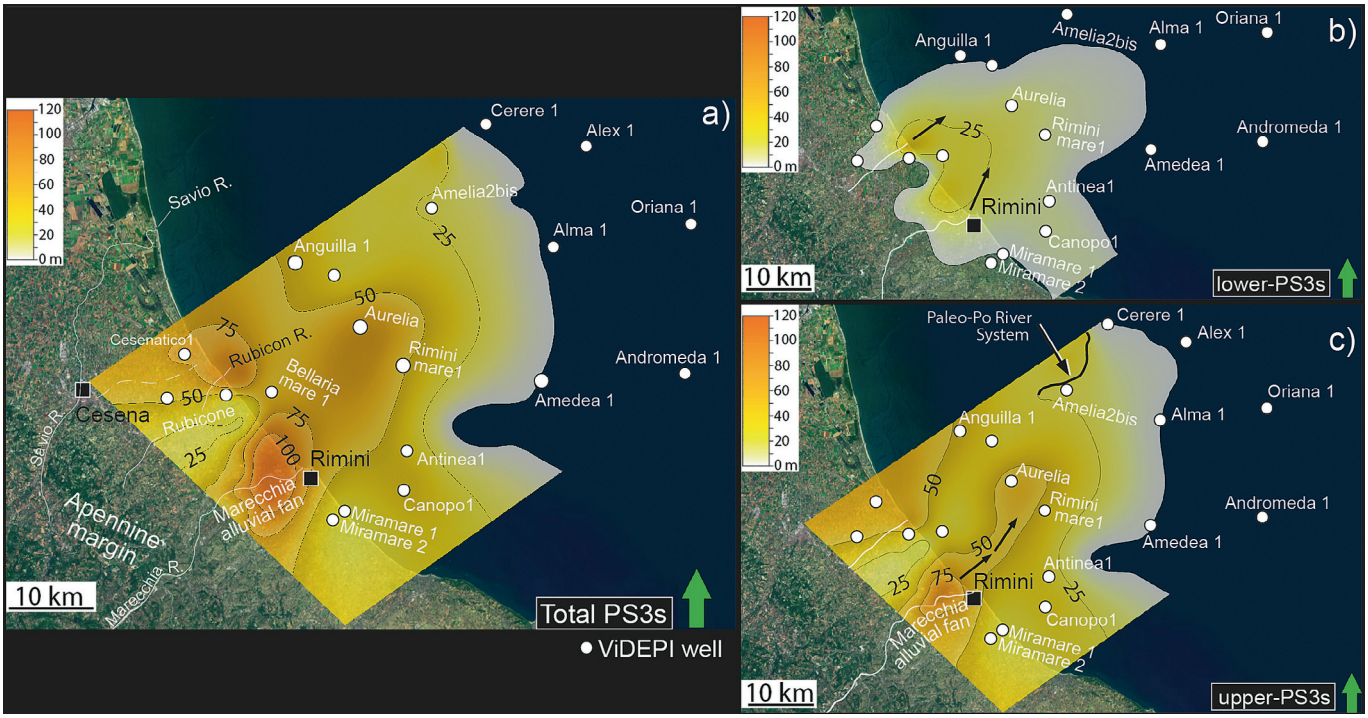

Fig. 8. Net thickness maps of freshwater aquifers. Net thickness maps (m) of aquifers containing fresh water (FW). (a) Total net thickness of FW aquifers across the study area. (b) Net thickness of FW aquifers in the lower-PS3 interval (870–450 kyr BP). (c) Net thickness of FW aquifers in the upper-PS3 interval (last 450 kyr). Savio R. = Savio River. Rubicon R. = Rubicon River. Marecchia R. = Marecchia River.

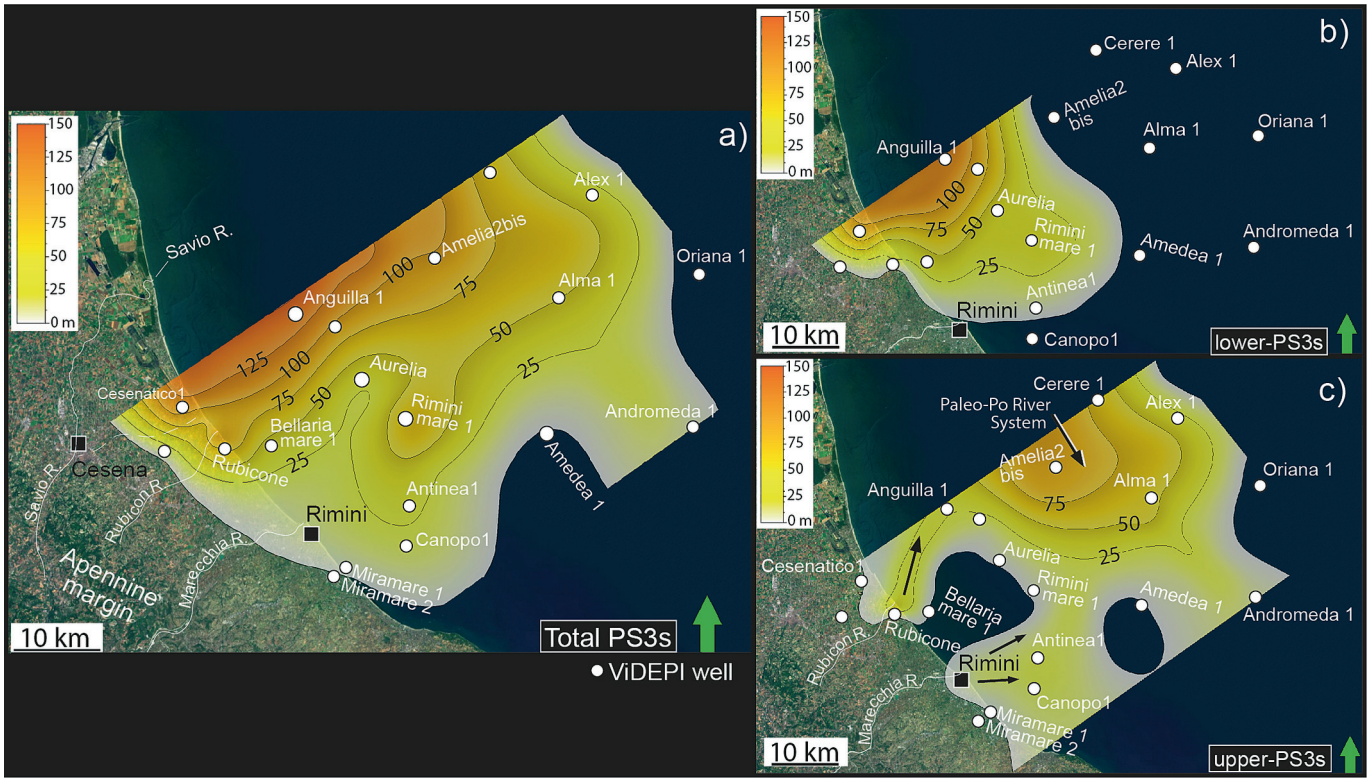

Fig. 9. Net thickness maps of brackish water aquifers. Net thickness maps (m) of aquifers containing brackish water (BW). (a) Total net thickness of BW aquifers across the study area. (b) Net thickness of BW aquifers in the lower-PS3 interval (870–450 kyr BP). (c) Net thickness of BW aquifers in the upper-PS3 interval (last 450 kyr BP). Savio R. = Savio River. Rubicon R. = Rubicon River. Marecchia R. = Marecchia River.

Table 2
Stored fresh (FW) and brackish (BW) pore water volume (V_p) assessed for the upper-, lower- and total PS3 sequence. Three different porosity ϕ (33%, 38% and 45%) scenarios were considered.

Unit	Bulk volume (km^3)	V_p, 33% ϕ (km^3)	V_p, 38% ϕ (km^3)	V_p, 45% ϕ (km^3)
FW upper-PS3s	59.3	19.6	22.5	26.7
FW lower-PS3s	10.6	3.5	4.0	4.8
FW total PS3s	**69.9**	**23.1**	**26.5**	**31.5**
BW upper-PS3s	51.7	17. 0	19.6	23.3
BW lower-PS3s	36.2	12.0	13.8	16.3
BW total PS3s	**87.9**	**29.0**	**33.4**	**39.6**

tor of the Adriatic shelf (Fig. 8c) during a certain sea-level lowstand phase caused by the glacio-eustatic forcing, consistently with the progradational dynamics documented for the Po system during the Last Glacial Maximum (Pellegrini et al., 2018).

The total bulk volume of FW aquifers is 69.9 km^3 (Table 2). Across the three porosity scenarios presented in Table 2, the total volume of FW stored beneath this sector of the Adriatic shelf (Fig. 8a) ranges from 23.1 to 31.5 km^3, relative to a baseline estimate of 26.5 km^3 at 38% porosity. Approximately, a volume of about 4 km^3 (min. 3.5 km^3 to max. 4.8 km^3) of fresh groundwater is contained in the lower-PS3 unit, whereas at least 22.5 km^3 (min. 19.6 km^3 to max. 26.7 km^3) is stored in the upper-PS3 unit (Table 2) but could be up to three times this volume.

4.4. Net thickness of brackish aquifers and pore water volumes assessment

Fig. 9 shows the total net thickness of the aquifer units including brackish water (BW) within the PS3s, as well as their areal extent throughout the Adriatic shelf and pore-water volumes. In line with Fig. 8, the maps of Fig. 9b and 9c display the total net thickness of BW aquifers within the lower- (870–450 kyr BP) and the upper-PS3 (last 450 kyr) units. The reader should consider the same underestimation discussed for the upper-PS3s due to the lack of data in the uppermost interval (Figs. 6 and 7).

The highest thickness values exceed 125 m and are documented for the northern sector, near the Anguilla1 well (Fig. 9a). Thickness values progressively decrease to the south and to the east toward the offshore sector, and to the west toward the modern coast (Fig. 9a). This configuration is coherent with the stratigraphic architecture (Figs. 6 and 7) and the onshore location of the freshwater recharging zone in proximity of the Apennine margin (Fig. 9). Similar BW extent is depicted in Fig. 9b (lower-PS3s), with up to 100 m-thick BW aquifers identified at the Anguilla1 well. On the other hand, Fig. 9c (upper-PS3s) shows a quite different configuration. The main depocenter, up to 75 m-thick, is located about 15 km offshore from the depocenter of Fig. 9b. During the last 450 kyr, BW aquifers likely migrated to the SE, reaching the location of Canopo1 well (Fig. 9c). Differently from the FW aquifers, no clear correlation exists with the modern alluvial fans of the Apennine river system. Only locally, a slight influence of the Apennine systems can be identified in correspondence of the Rubicon and Marecchia alluvial fans (Fig. 9c). Here, onshore-offshore elongated aquifer units, less than 25 m thick, seem to merge with the southward-directed Po system, as discussed above. Differently from the lower-PS3 interval, where the offshore BW aquifer systems appear disconnected with the onshore recharging area (Fig. 6b), the hydrostratigraphic reconstruction for the upper-PS3 suggests potential connection with the landward systems and possible active recharge for these aquifers (Figs. 6 and 7).

The total volume of BW aquifers is about 87.9 km^3 (Table 2). For these aquifers, estimated BW volume ranges from 29.0 to 39.6 km^3, compared to the mean value of 33.4 km^3 at 38% of porosity (Table 2). Approximately, 13.8 km^3 of these are stored in the lower-PS3s (min. 12.0 km^3 to max. 16.3 km^3), and 19.8 km^3 in the upper-PS3s (min. 17.0 km^3 to max. 23.3 km^3; Table 2).

4.5. Hydrogeological model

A simple scoping double-density analytical model was used to test whether the offshore freshwater aquifers are still actively recharged by the permeable alluvial units outcropping onshore (Figs. 1, 6 and 7) and whether the geometric and petrophysical properties of the aquifers can explain the freshwater-saltwater distribution on the shelf, as shown in Figs. 6 and 7. We have tested several aquifer geometries that were compatible with those represented in Fig. 6. The model has been initially applied to the aquifer complexes within PS2s, lower- and upper-PS3, separately, using the three major unconformities (PS2u, PS3u, and PS3ub of Fig. 6) as aquifer boundaries. The results of these simulations, however, have not been satisfactory, because the aquifer recharge and hydraulic conductivity values required to match the observed geometries were not realistic. This is probably due to the three basal unconformities not being hydraulic boundaries, especially at the Apennine margin, where they *de facto* consist of erosional surfaces. On the other hand, when evaluating the three aquifer complexes together, the freshwater-saltwater distribution observed has been satisfactorily modelled. The results are shown in Fig. 10. The horizontal flow rate obtained for the offshore sector of the transects corresponds to an aquifer recharge of 250 mm/year. This value is consistent with the current recharge estimates in the area (Severi et al., 2014; Antonellini et al., 2015). Most aquifers confined between aquitards/aquicludes exhibit horizontal rather than vertical connection and can extend inland, as documented in Figs. 6 and 7. Under this configuration, and given the dominance of horizontal flow, the combined PS2s + PS3s package behaves as a single hydrostratigraphic unit, balancing seawater intrusion with offshore-directed freshwater flow (q_0 in Fig. 10). These results suggest that most of the offshore aquifers, those directly linked to onshore systems, are still actively recharged by their exposed counterparts along the Apennine margin, in proximity to the modern alluvial fans of the Marecchia and Savio rivers (Fig. 8).

5. Discussion

5.1. The OFG Po-Adriatic volume revealed

The coastal-to-shelf mapping of the PS3s aquifers has shown that the aquifer bodies of the lower- and upper-PS3s are the offshore equivalents of aquifer groups B and A, respectively (Figs. 2 and 11a-b). The latter are currently exploited for agricultural, industrial, and domestic purposes (Regione Emilia-Romagna and Eni-Agip, 1998; Regione Lombardia and Eni-Divisione Agip, 2002). The PS2s includes the offshore counterpart of aquifer group C but does not contain any fresh groundwater (Figs. 6, 7 and 11a-b). Compared with previous studies

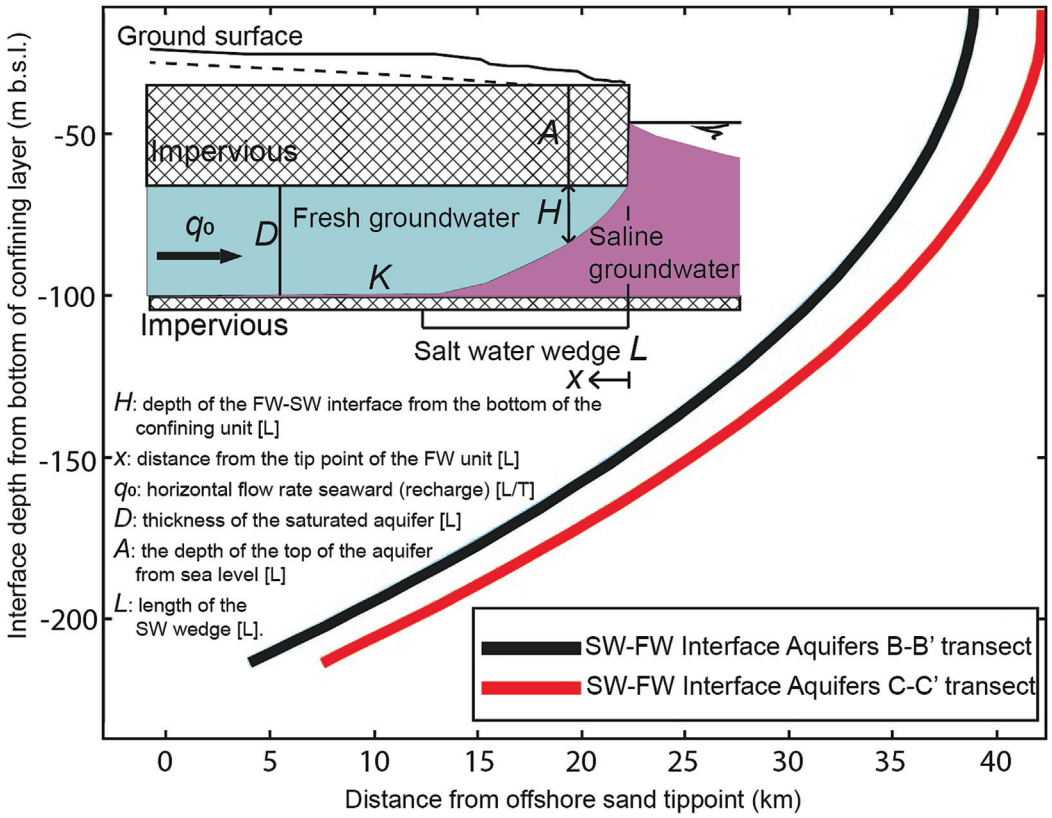

Fig. 10. Model of the freshwater-saltwater interface in offshore aquifer systems. Position of the freshwater-saltwater interface along the hydrostratigraphic transects of Fig. 6, expressed relative to the base of the confining layer and derived from the analytical model of Oude Essink (2000). The inset (modified after Oude Essink, 2000) illustrates the main components of the model.

that either lacked offshore salinity data (Lofi et al., 2013b; Campo et al., 2024) or documented only brackish to saline groundwater (Giustiniani et al., 2022) and scattered low-salinity (<25,000 mg/L) bodies south of the modern Po Delta (Giustiniani et al., 2022), our study provides a significant step forward by demonstrating the presence of important offshore freshwater volumes within the Adriatic shelf. Considering mean volume estimates at 38% of porosity, about 26.5 km^3 of fresh water are contained in this shallow (uppermost 300 m) and multi-layered aquifer system within the first 35 km from the Italian coast (Fig. 8; Table 2). An additional 33.4 km^3 of brackish water are available, extending the radius up to 15 km basinward and 100 m downward beneath the seabed (Figs. 6 and 9). Despite the lack of shallow data, based on the typology of aquifer deposits and their thickness trends (Figs. 8-9), fresh water and brackish water volumes contained within the upper-PS3 unit could exceed 60 km^3 and 55 km^3, respectively. For both FW and BW aquifers, sensitivity analysis results demonstrate that a ±5%–7% variation in porosity produces volumetric changes of approximately ±13%–20%. The conservative scenario (33% porosity, Table 2) yielded values 13%–15% lower, whereas the optimistic scenario (45% porosity, Table 2) yielded values 18%–20% higher, relative to the mean estimate at 38% porosity. Hence, porosity uncertainty is a first-order control on volumetric estimates, but it does not alter the overall distribution or relative proportions between freshwater and brackish water resources. This analysis demonstrates that, although absolute groundwater storage depends on the adopted porosity value, the relative differences among aquifer units, as well as their overall volumetric hierarchy, remain unchanged across the tested porosity range. Consequently, the volumetric interpretation presented in this study is robust with respect to reasonable porosity variability.

In a coastal sector where available freshwater reserves are overexploited and already threatened by climate change effects (Antonioli et al., 2017; Mastrocicco et al., 2019), the identification of such untapped and unconventional reserves could raise awareness among citizens and policymakers of the importance of this strategic resource, which could be used to alleviate forthcoming and increasingly severe water crises (Bakken et al., 2012; Pascale and Ragone, 2025). We acknowledge that water quality may be lower than that required for drinking purposes under Directive (EU) 2020/2184 of European Parliament and the Council of European Union (2020). However, such resources could be rendered potable after minor treatment, or alternatively, used as cost-effective raw source of water for desalinization (Sheng et al., 2023). Although offshore aquifer exploitation is, at present, "not in the planning", and its economic viability remains uncertain (Zamrsky et al., 2024b), largely due to existing technological limitations (Micallef et al., 2021), the North Adriatic aquifers represent an excellent target for further investigations. Future work should include direct sampling to assess groundwater quality, as well as isotopic and hydrodynamic analyses to quantify the proportion of offshore volumes actively recharged from inland areas. Both the low salinity and the limited burial depth of these aquifers may substantially reduce the costs and the environmental impact associated with exploration and potential exploitation, particularly when compared with other deeper offshore groundwater bodies (Horozal et al., 2025) or with smaller, low-salinity coastal-to-shelf systems along the Mediterranean coasts (Chiacchieri et al., 2025). In addition, the presence of offshore hydrocarbon platforms (Fig. 1) that will soon be decommissioned, offers a timely opportunity for cost-effective repurposing and prompt further investigation. The reuse of existing offshore infrastructure may additionally reduce the costs associated with exploration and monitoring of offshore aquifers, as shown by a feasibility plan funded by the BluMed initiative (Antoncecchi et al., 2020).

5.2. Drivers of offshore freshened groundwater formation

The well-constrained chronological framework available for the Po-Adriatic system allowed investigation of the different roles played by tectonics and glacio-eustasy, which are the main factors controlling the distribution and emplacement of offshore fresh groundwater (OFG; Micallef et al., 2021). The two most recent episodes of Apennine uplift are dated to approximately 870 kyr BP and 450 kyr BP, respectively (Regione Emilia-Romagna and Eni-Agip, 1998). The onset of the glaciations with a 100 kyr cyclicity (Muttoni et al., 2003), is also established at about 870 kyr BP. Therefore, the lower-PS3s record superimposed effects of both tectonics and glacio-eustasy between 870–450 kyr BP. Conversely, given the post-450 kyr BP tectonic stasis, the accumulation of the upper-PS3s offshore aquifers can be primarily ascribed to glacio-eustatic variations.

At the Apennine margin, in proximity of the alluvial fans, the two latest uplifting events increased the topographic gradient and triggered erosional processes that formed the unconformities PS3 and PS3b (Fig. 11a). Consequently, meteoric freshwater could progressively move from the recharge areas toward the marine PS2s aquifers and offshore through both the lower and upper-PS3s aquifers (Fig. 11a-b). The PS3 unconformity (PS3u) marks the onset of tectonically driven NE-directed shift of the Apennine Complex, with the shelf/slope limit progressively migrating basinward (Ghielmi et al., 2013), from about 17 km up to 35 km from the modern coastline (Fig. 6). This limit also represents the maximum offshore extent of fresh water within the PS3s aquifers.

Besides tectonics, superimposed 100 kyr glacio-eustatic cycles played a crucial role in delivering large volumes of coarse-grained sediment delivered to the shelf after glaciations (Vandenberghe, 2003; Ghielmi et al., 2013), but also for the development of the multi-layered structure of the PS3s aquifer systems (Figs. 6 and 7). The latter are characterized by vertically-stacked marine and continental deposits that parallel the cyclic arrangement of facies of the Middle-Pleistocene Po-Plain succession linked to glacio-eustatic oscillations (Ridente et al., 2008; Bruno et al., 2024). The alternation of laterally continuous fine-grained (i.e., aquitards/aquicludes) and coarse-grained intervals (i.e., aquifers) allowed the basinward distributions of groundwater, whereas permeability barriers limit vertical exchanges. High amalgamation of aquifers bodies, along with their pronounced lateral connectivity and continuity, is also attributed to glacial lowstands, when the continental shelves were subaerially exposed and river systems merged into larger trunk channels (Sømme et al., 2009; Blum et al., 2013; Pellegrini et al., 2017b). During these phases, and provided sufficient sediment supply, fluvio-deltaic systems prograded to the shelf-edge (Blum and Törnqvist, 2000; Carvajal et al., 2009; Pellegrini et al., 2018). Such basinward progradation likely promoted the migration of connate, deposition-time saline water toward the basin, as illustrated in Fig. 11c. The enhanced hydraulic gradient caused by the stepwise sea-level drop (T1, T2 and T3 – Fig. 11c), would have facilitated the basinward migration of fresh water through the prograding fluvial network over multiple glacial cycles (Fig. 10c). Subsequent deposition of mud-dominated strata during sea-level rise and highstand formed thick, laterally extensive permeability barriers, as shown by Campo et al. (2024) for the post-LGM succession in the Central Adriatic. These permeability barriers compartmentalized coarse-grained bodies, thereby enhancing the preservation of fresh and brackish water.

5.3. Beneath the shelf: decoding the control exerted by the stratigraphic setting

The stratigraphic setting resulting from the interplay between tectonics and glacio-eustasy drives both the distribution and preservation of fresh-to-brackish groundwater beneath the Adriatic shelf. Our onshore-offshore reconstruction showed that PS3s aquifers extend up to 50 km, mostly continuously, from the subsurface of the modern coast and down to the shelf (Figs. 6–9). Their thickness and areal extent reflect the long-term progradational trend of the PS3s, driven by progressive basin filling and shelf-slope migration toward NE over the last 870 kyr (Amadori et al., 2019). Consequently, the upper-PS3s become increasingly dominated by continental deposits, with laterally continuous fluvio-deltaic strata forming the main offshore aquifers (Figs. 6, 7 and 11a-b). These units grade laterally into alluvial fan gravels in proximal settings and into deltaic-to-coastal sediments in more distal sectors, with mud content increasing down-section (Figs. 6 and 7). This architectural motif is consistent with established fluvio-deltaic models (Gani and Bhattacharya, 2005; Nichols and Fisher, 2007; Miall, 2013) and supports the occurrence spatial continuity of fresh groundwater throughout multiple sectors of the shelf (Fig. 11a-b). Where hydraulic gradients are favourable, groundwater can migrate seaward through these permeable fluvial units, maintaining hydraulic (horizontal) continuity between onshore and offshore aquifer systems (Fig. 11a-b), as also observed in other continental-shelf settings (Burnett et al., 2006; Cohen et al., 2010; Person et al., 2018; Gustafson et al., 2019; Attias et al., 2021). The widespread presence of fresh water within the upper-PS3s (Figs. 6 and 7) is therefore directly linked to the dominance of laterally continuous fluvio-deltaic facies, which provide both high porosity and strong connectivity. Overall, the highest fresh pore-water content is where the offshore aquifers are directly connected to onshore alluvial fans. Thus, our results show that one of the main factors controlling the emplacement of fresh groundwater within offshore aquifers is their direct stratigraphic and hydraulic connection with the onshore alluvial fan systems, which represent key zones of active recharge (Fig. 11a). This connection also controls freshwater emplacement in the deeper PS2s aquifers. Although these units are of marine origin, localized fresh water has been detected beneath the southern coastal sector (Fig. 11a). Here, the PS3 erosional unconformity provides a direct linkage with overlying alluvial fan gravels, while tectonic uplift enhances the topographic gradient. These conditions likely favoured the progressive flushing of connate salt water and its replacement by meteoric water infiltrating near the Apennine margin (Fig. 11a). In contrast, no fresh water is observed northward, where PS2s and lower-PS3s aquifers are disconnected from inland recharge areas and where the gentler topographic gradient reduces the potential for meteoric infiltration (Fig. 11b).

5.4. Offshore aquifers: hidden reserves or fossil relics?

The reconstructed OFG distribution is strongly supported by the hydrogeological model presented in Fig. 10. To maintain the fresh-to-salty water interfaces shown by the hydrostratigraphic transects, an active meteoric recharge of approximately 250 mm/yr is required. Locally, within specific stratigraphic intervals and restricted areas, some offshore aquifers appear to be disconnected from onshore recharge zones. As a result, these units cannot benefit from rainfall or artificial recharge (Fig. 11a), and their pore waters should be regarded as non-renewable, or "fossil", resources (Fig. 11b). Fossil groundwater is predominantly connate — i.e., trapped during aquifer deposition — and its salinity generally reflects the original depositional environment: freshwater in fluvial settings, brackish in back-barrier systems, and saline in marine deposits (GebreEgziabher et al., 2022). From a sustainability perspective, such fossil water bodies should not be considered viable targets for future exploitation. This evidence highlights how integrated onshore-offshore investigations enable the identification of alternative groundwater resources, while also emphasizing the need to distinguish renewable, actively recharged systems from

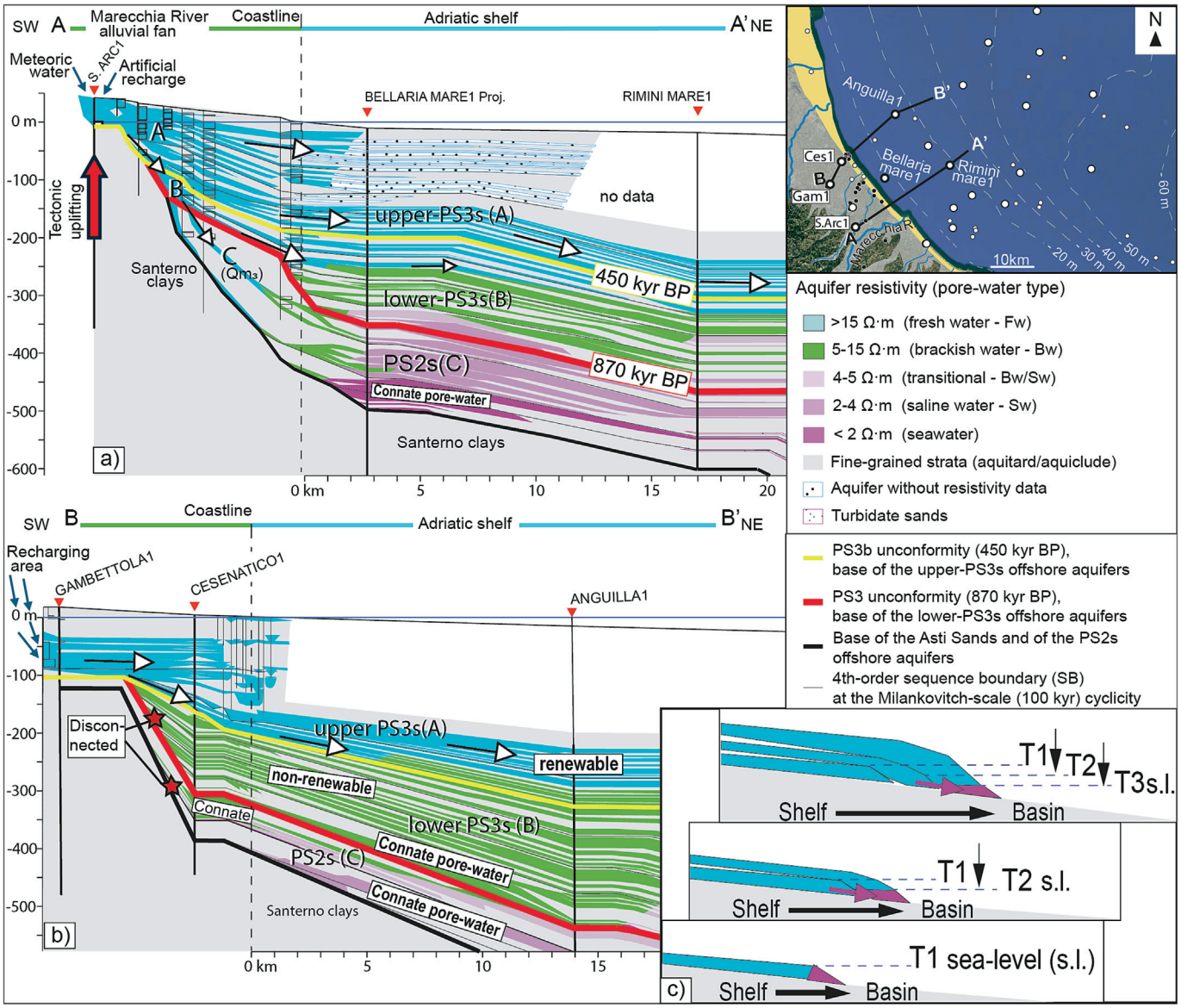

Fig. 11. Mechanisms of OFG distribution and emplacement. Scaled-up views of the hydrostratigraphic transects C-C' and A-A' (the location of the transects is shown in the upper-right map) to illustrate the main factors controlling the distribution and emplacement of fresh and brackish groundwater beneath the Northern Adriatic shelf. (a) Scaled-up view of transect C-C' (Fig. 6b). Blue arrows indicate meteoric or anthropogenic recharge from the onshore sector, whereas white arrows illustrate main groundwater flow pathways. (b) Scaled-up view of transect A-A' (Fig. 7a). Red stars mark aquifers that are disconnected from onshore recharge zones and are therefore interpreted as non-renewable resources. (c) Simplified conceptual model illustrating the impact of stepwise sea-level falls during glacial periods, which promote progressive connate saltwater removal (purple arrows) and subsequent freshwater emplacement within the fluvial systems prograding across the exposed shelf. (A), (B) and (C) correspond to the onshore aquifer groups shown in Fig. 2. Proj. = projected well.

fossil, non-renewable ones. Beyond the implications for offshore groundwater utilization, improving freshwater storage beneath modern coastal areas — peculiarly where artificial recharge is already employed — may greatly benefit from recognizing and assessing the offshore extension of onshore aquifer systems.

6. Conclusions

Reinterpretation of legacy stratigraphic, geophysical, hydrogeological, and geochemical datasets, integrated with coastal-to-shelf well-logs correlation, salinity classification, volumetric analysis, and first-order hydrogeological modelling, enabled the identification and quantification of offshore fresh and brackish groundwater beneath the North Adriatic shelf. Freshwater and brackish water occur within laterally extensive, multi-layered fluvio-deltaic aquifers of the PS3 Sequence (last ~870 kyr), extending up to ~50 km offshore within the upper ~400 m below the seafloor. Minimum estimated volumes reach 26.5 km^3 of fresh water and 33.4 km^3 of brackish water.

Coastal-to-shelf correlations demonstrate that offshore aquifers represent the basinward continuation of onshore groundwater systems, with net-thickness patterns indicating strong lateral connectivity developed during repeated lowstand shelf exposure and fluvio-deltaic progradation and deposition over multiple glacial-interglacial cycles during the last 870 kyr.

The distribution and long-term preservation of low-salinity offshore groundwater are primarily controlled by Pleistocene glacio-eustatic oscillations, tectonic activity, and the development of regionally extensive aquitards during transgressive and highstand phases.

Hydrogeological evidence and modelling consistently support active hydraulic connectivity and a land-to-sea freshwater flow regime, implying that a significant portion of these offshore resources is actively recharged and potentially renewable.

Despite the need for further validation and water-quality assessment, the shallow depth, large areal extent, and relatively low salinity of these aquifers highlight their potential relevance for future resource evaluation. More broadly, this study demonstrates that legacy hydrocarbon and groundwater datasets provide a transferable, cost-effective framework for offshore groundwater assessment in continental-shelf settings worldwide.

7. Materials availability

The two open-source datasets analysed in this work are available at the following links:

- ViDEPI Project at https://www.videpi.com/videpi/pozzi/consultabili.asp
- Geological Survey of Regione Emilia-Romagna at https://ambiente.regione.emilia-romagna.it/it/geologia/servizi-e-strumenti/cartografie-webgis/prove-geognostiche-e-geotecniche-1

CRediT authorship contribution statement

Bruno Campo: Writing – original draft, Methodology, Investigation, Formal analysis, Data curation, Conceptualization. **Marco Antonellini:** Writing – review & editing, Validation, Software, Formal analysis. **Claudio Pellegrini:** Writing – review & editing.

Declaration of competing interest

The authors declare that they have no known competing financial interests or personal relationships that could have appeared to influence the work reported in this paper.

Acknowledgements

The authors gratefully acknowledge Schlumberger for the generous donation of the Petrel software package to the University of Bologna. We also express sincere thanks to Prof. Alessandro Amorosi (Università di Bologna) for his longstanding scientific guidance, which has been instrumental in shaping the authors' research approach, and for facilitating access to the Schlumberger Petrel software employed in this study.

Appendix A. Supplementary data

Supplementary data to this article can be found online at https://doi.org/10.1016/j.gsf.2026.102286.

References

Amadori, C., Toscani, G., Di Giulio, A., Maesano, F.E., D'Ambrogi, C., Ghielmi, M., Fantoni, R., 2019. From cylindrical to non-cylindrical foreland basin: Pliocene–Pleistocene evolution of the Po Plain–Northern Adriatic basin (Italy). Basin Res. 31, 991–1015. https://doi.org/10.1111/bre.12369.

Amorosi, A., Colalongo, M.L., 2005. The linkage between alluvial and coeval nearshore marine successions: evidence from the Late Quaternary record of the Po River Plain, Italy. In: Blum, M.D., Marriott, S.B., Leclair, S.F. (Eds.), Fluvial Sedimentology VII. IAS Spec. Publ. 35, 257–275. doi:10.1002/9781444304350.ch15.

Amorosi, A., Maselli, V., Trincardi, F., 2016. Onshore to offshore anatomy of a late Quaternary source-to-sink system (Po Plain-Adriatic Sea, Italy). Earth-Sci. Rev. 153, 212–237. https://doi.org/10.1016/j.earscirev.2015.10.010.

Amorosi, A., Pavesi, M., 2010. Aquifer stratigraphy from the Middle–Late Pleistocene succession of the Po Basin. Mem. Descr. Carta Geol. D'it. 15, 7–20.

Amorosi, A., Pavesi, M., Ricci Lucchi, M., Sarti, G., Piccin, A., 2008. Climatic signature of cyclic fluvial architecture from the Quaternary of the central Po Plain, Italy. Sediment. Geol. 209, 58–68. https://doi.org/10.1016/j.sedgeo.2008.06.010.

Amorosi, A., Colalongo, M.L., Fiorini, F., Fusco, F., Pasini, G., Vaiani, S.C., Sarti, G., 2004. Palaeogeographic and palaeoclimatic evolution of the Po Plain from 150 kyr core records. Global Planet. Change 40, 55–78. https://doi.org/10.1016/S0921-8181(03)00098-5.

Amorosi, A., Farina, M., Severi, P., Preti, D., Caporale, L., Di Dio, G., 1996. Genetically related alluvial deposits across active fault zones: an example of alluvial fan–terrace correlation from the upper Quaternary of the southern Po Basin, Italy. Sediment. Geol. 102, 275–295. https://doi.org/10.1016/0037-0738(95)00074-7.

Amorosi, A., Colalongo, M.L., Fusco, F., Pasini, G., Fiorini, F., 1999. Glacio-eustatic control of continental–shallow marine cyclicity from Late Quaternary deposits of the southeastern Po Plain, northern Italy. Quaternary Res. 52, 1–13. https://doi.org/10.1006/qres.1999.2049.

Angrilli, M., 2024. From Floating Architecture to Seaside Landscape: The Case of the Island. In: Proc. Third World Conference on Floating Solutions (WCFS 2023). Springer, pp. 269. doi:10.1007/978-981-97-0495-8_16.

Antoncecchi, I., Rossi, G., Bevilacqua, M., Cianella, R., Vico, G., Ferrero, S., Catania, F., Pacini, M., Mondelli, N., Rovere, M., Bibuli, M., 2020. Research hub for an integrated green energy system reusing sealines for H_2 storage and transport. Environ. Eng. Manage. J. 19, 10.

Antonellini, M., Mollema, P., Giambastiani, B., Bishop, K., Caruso, L., Minchio, A., Pellegrini, L., Sabia, M., Ulazzi, E., Gabbianelli, G., 2008. Salt water intrusion in the coastal aquifer of the southern Po Plain, Italy. Hydrogeol. J. 16, 1541–1556. https://doi.org/10.1007/s10040-008-0319-9.

Antonellini, M., Allen, D.M., Mollema, P.N., Capo, D., Greggio, N., 2015. Groundwater freshening following coastal progradation and land reclamation of the Po Plain, Italy. Hydrogeol. J. 23, 1009–1026. https://doi.org/10.1007/s10040-015-1263-0.

Antonioli, F., Anzidei, M., Amorosi, A., Presti, V.L., Mastronuzzi, G., Deiana, G., De Falco, G., Fontana, A., Fontolan, G., Lisco, S., Marsico, A., 2017. Sea-level rise and potential drowning of the Italian coastal plains: flooding risk scenarios for 2100. Quaternary Sci. Rev. 158, 29–43. https://doi.org/10.1016/j.quascirev.2016.12.021.

Attias, E., Constable, S., Sherman, D., Ismail, K., Shuler, C., Dulai, H., 2021. Marine electromagnetic imaging and volumetric estimation of freshwater plumes offshore Hawai'i. Geophys. Res. Lett. 48, e2020GL091249. https://doi.org/10.1029/2020GL091249.

Azienda Generale Italiana Petroli Mineraria, 1959. Atti del Convegno su Giacimenti Gassiferi dell'Europa Occidentale, Milano, 30 September–5 October 1957. Accademia Nazionale dei Lincei ed Ente Nazionale Idrocarburi, Roma, vol. 2, p. 45-49 (in Italian).

Bakken, T.H., Ruden, F., Mangset, L.E., 2012. Submarine groundwater: a new concept for the supply of drinking water. Water Resour. Manag. 26, 1015–1026. https://doi.org/10.1007/s11269-011-9806-1.

Bertolini, G., Cazzoli, M.A., Centineo, M.C., Cibin, U., Martini, A., 2008. Emilia-Romagna Geological Landscape Map, 1:250,000 scale. https://ambiente.regione.emilia-romagna.it/en/geologia/geology/geological-heritage/geological-landscape-new.

Bhattacharya, J.P., 2006. Deltas. SEPM Spec. Publ. 84, 237–292. https://doi.org/10.2110/pec.06.84.0237.

Blum, M., Martin, J., Milliken, K., Garvin, M., 2013. Paleovalley systems: Insights from Quaternary analogs and experiments. Earth-Sci. Rev. 116, 128–169. https://doi.org/10.1016/j.earscirev.2012.09.003.

Blum, M.D., Törnqvist, T.E., 2000. Fluvial responses to climate and sea-level change: a review and look forward. Sedimentology 47, 2–48. https://doi.org/10.1046/j.1365-3091.2000.00008.x.

Boccaletti, M., Corti, G., Martelli, L., 2011. Recent and active tectonics of the external zone of the Northern Apennines (Italy). Int. J. Earth Sci. 100, 1331–1348. https://doi.org/10.1007/s00531-010-0545-y.

Bonaldo, D., Bellafiore, D., Ferrarin, C., Ferretti, R., Ricchi, A., Sangelantoni, L., Vitelletti, M.L., 2023. The summer 2022 drought: a taste of future climate for the Po valley (Italy)? Reg. Environ. Change 23 (1). https://doi.org/10.1007/s10113-022-02004-z.

Briggs, I.C., 1974. Machine contouring using minimum curvature. Geophysics 39 (1), 39–48. https://doi.org/10.1190/1.1440410.

Bruno, L., Demurtas, L., Magri, D., Michelangeli, F., Rittenour, T., Hong, W., Rossi, V., Vaiani, S.C., Vecchi, A., Amorosi, A., 2024. Sedimentary response of the Po Basin to Mid–Late Pleistocene glacio-eustatic oscillations. Quat. Sci. Rev. 344, 109005. https://doi.org/10.1016/j.quascirev.2024.109005.

Burnett, W.C., Aggarwal, P.K., Aureli, A., Bokuniewicz, H., Cable, J.E., Charette, M.A., Kontar, E., Krupa, S., Kulkarni, K.M., Loveless, A., Moore, W.S., 2006. Quantifying submarine groundwater discharge in the coastal zone via multiple methods. Sci. Total Environ. 367, 498–543. https://doi.org/10.1016/j.scitotenv.2006.05.009.

Campo, B., Antonellini, M., 2024. Offshore freshened groundwater reserves identification as revealed by geophysical and stratigraphic data: insights from the Northern Adriatic shelf (Italy). EGU General Assembly 2024, Vienna, Austria, 14–19 Apr 2024, EGU24-5599. https://10.5194/egusphere-egu24-5599.

Campo, B., Bohacs, K.M., Amorosi, A., 2020. Late Quaternary sequence stratigraphy as a tool for groundwater exploration: lessons from the Po River Basin (northern Italy). AAPG Bull. 104, 681–710. https://doi.org/10.1306/06121918116.

Campo, B., Pellegrini, C., Sammartino, I., Trincardi, F., Amorosi, A., 2024. New perspectives on offshore groundwater exploration through integrated sequence-stratigraphy and source-to-sink analysis: insights from the late Quaternary succession of the western Central Adriatic system, Italy. Earth-Sci. Rev. 256, 104880. https://doi.org/10.1016/j.earscirev.2024.104880.

Carminati, E., Doglioni, C., 2012. Alps vs. Apennines: the paradigm of a tectonically asymmetric Earth. Earth-Sci. Rev. 112, 67–96. https://doi.org/10.1016/j.earscirev.2012.02.004.

Carminati, E., Doglioni, C., Scrocca, D., 2003. Apennines subduction-related subsidence of Venice (Italy). Geophys. Res. Lett. 30 (13), 1717. https://doi.org/10.1029/2003GL017001.
Carvajal, C., Steel, R., Petter, A., 2009. Sediment supply: the main driver of shelf-margin growth. Earth-Sci. Rev. 96, 221–248. https://doi.org/10.1016/j.earscirev.2009.06.008.
Cattaneo, A., Correggiari, A., Langone, L., Trincardi, F., 2003. The late-Holocene Gargano subaqueous delta, Adriatic shelf: sediment pathways and supply fluctuations. Mar. Geol. 193, 61–91. https://doi.org/10.1016/S0025-3227(02)00614-X.
Cattaneo, A., Trincardi, F., Asioli, A., Correggiari, A., 2007. The Western Adriatic shelf clinoform: energy-limited bottomset. Cont. Shelf Res. 27, 506–525. https://doi.org/10.1016/j.csr.2006.11.013.
Catuneanu, O., Abreu, V., Bhattacharya, J.P., Blum, M.D., Dalrymple, R.W., Eriksson, P.G., Fielding, C.R., Fisher, W.L., Galloway, W.E., Gibling, M.R., Giles, K.A., 2009. Towards the standardization of sequence stratigraphy. Earth-Sci. Rev. 92, 1–33. https://doi.org/10.1016/j.earscirev.2008.10.003.
Chiacchieri, D., Lipparini, L., Jordan, E.Q., Bencini, R., Micallef, A., 2025. Coastal fresh groundwater extending deep offshore from southern Sicily (Italy): assessment of the Ragusa Aquifer via petrophysical and 3D hydrogeological modelling. Hydrogeol. J. (in press). https://doi.org/10.1007/s10040-025-02965-5.
Clark, P.U., Dyke, A.S., Shakun, J.D., Carlson, A.E., Clark, J., Wohlfarth, B., Mitrovica, J.X., Hostetler, S.W., McCabe, A.M., 2009. The last glacial maximum. Science 325, 710–714. https://doi.org/10.1126/science.1172873.
Clark, P.U., Shakun, J.D., Rosenthal, Y., Köhler, P., Bartlein, P.J., 2024. Global and regional temperature change over the past 4.5 million years. Science 383, 884–890. https://doi.org/10.1126/science.adi1908.
Cohen, D., Person, M., Wang, P., Gable, C.W., Hutchinson, D., Marksamer, A., Dugan, B., Kooi, H., Groen, K., Lizarralde, D., Evans, R.L., 2010. Origin and extent of fresh paleowaters on the Atlantic continental shelf, USA. Groundwater 48, 143–158. https://doi.org/10.1111/j.1745-6584.2009.00627.x.
Corradin, C., Thomas, A.T., Camerlenghi, A., Zini, L., Giustiniani, M., Busetti, M., Foglia, L., Bertoni, C., Micallef, A., 2025. Characterization of an onshore–offshore aquifer system in the Venetian Friulian Plain and north Adriatic Basin: a 3D modeling approach. Hydrogeol. J. https://doi.org/10.1007/s10040-025-02952-w (in press).
Correggiari, A., Cattaneo, A., Trincardi, F., 2005. The modern Po Delta system: lobe switching and asymmetric prodelta growth. Mar. Geol. 222, 49–74. https://doi.org/10.1016/j.margeo.2005.06.039.
Custodio, E., 2002. Aquifer overexploitation: what does it mean? Hydrogeol. J. 10, 254–277. https://doi.org/10.1007/s10040-002-0188-6.
Custodio, E., 2010. Coastal aquifers of Europe: an overview. Hydrogeol. J. 18, 269–280. https://doi.org/10.1007/s10040-009-0496-1.
Dalla, S., Rossi, M., Orlando, M., Visentin, C., Gelati, R., Gnaccolini, M., Papani, G., Belli, A., Biffi, U., Citrullo, D., 1992. Late Eocene-Tortonian tectono-sedimentary evolution in the western part of the Padan Basin (northern Italy). Paleontol. Evol. 24–25, 34–1362.
Dondi, L., D'Andrea, M.G., 1986. La Pianura Padana e Veneta dall'Oligocene superiore al Pleistocene. G. Geol. Ser. 48 (1–2), 197–225 (in Italian).
European Parliament and the Council of European Union, 2020. Directive 2020/2184 of the European Parliament and of the Council of 16 December 2020 on the quality of water intended for human consumption. Official Journal of the European Union L 435, 1–62. https://eur-lex.europa.eu/eli/dir/2020/2184/oj.
Ferranti, L., Antonioli, F., Mauz, B., Amorosi, A., Dai Pra, G., Mastronuzzi, G., Monaco, C., Orrù, P., Pappalardo, M., Radtke, U., Renda, P., Romano, P., Sanso, P., Verrubbi, V., 2006. Markers of the last interglacial sea-level high stand along the coast of Italy: tectonic implications. Quat. Int. 145-146, 30–54. https://doi.org/10.1016/j.quaint.2005.07.009.
Fetter, C.W., 2014. Applied Hydrogeology. Pearson, Harlow, p. 610.
Fontana, A., Mozzi, P., Bondesan, A., 2010. Late Pleistocene evolution of the Venetian-Friulian plain. Rend. Lincei 21, 181–196. https://doi.org/10.1007/s12210-010-0093-1.
Gani, M.R., Bhattacharya, J.P., 2005. Lithostratigraphy versus chronostratigraphy in facies correlations of Quaternary deltas: application of bedding correlation. In: Giosan, L., Bhattacharya, J.P. (Eds.), River Deltas: Concepts, Models, and Examples. SEPM Spec. Publ. 83, 31-48. doi:10.2110/pec.05.83.0031.
Garzanti, E., Vezzoli, G., Andò, S., 2011. Paleogeographic and paleodrainage changes during Pleistocene glaciations (Po Plain, northern Italy). Earth-Sci. Rev. 105, 25–48. https://doi.org/10.1016/j.earscirev.2010.11.004.
Geach, M.R., Stokes, M., Telfer, M.W., Mather, A.E., Fyfe, R.M., Lewin, S., 2014. The application of geospatial interpolation methods in the reconstruction of Quaternary landform records. Geomorphology 216, 234–246. https://doi.org/10.1016/j.geomorph.2014.03.036.
GebreEgziabher, M., Jasechko, S., Perrone, D., 2022. Widespread and increased drilling of wells into fossil aquifers in the USA. Nat. Commun. 13, 2129. https://doi.org/10.1038/s41467-022-29678-7.
Ghielmi, M., Minervini, M., Nini, C., Rogledi, S., Rossi, M., Vignolo, A., 2010. Sedimentary and tectonic evolution in the eastern Po-Plain and northern Adriatic Sea area from Messinian to Middle Pleistocene (Italy). Rend. Lincei 21 (Suppl. 1), 131–166.
Ghielmi, M., Minervini, M., Nini, C., Rogledi, S., Rossi, M., 2013. Late Miocene–Middle Pleistocene sequences in the Po Plain–Northern Adriatic Sea (Italy): the stratigraphic record of modification phases affecting a complex foreland basin. Mar. Petrol. Geol. 42, 50–81. https://doi.org/10.1016/j.marpetgeo.2012.11.007.
Giambastiani, B.M., Antonellini, M., Oude Essink, G.H., Stuurman, R.J., 2007. Saltwater intrusion in the unconfined coastal aquifer of Ravenna (Italy): a numerical model. J. Hydrol. 340 (1–2), 91–104. https://doi.org/10.1016/j.jhydrol.2007.04.001.
Giambastiani, B.M.S., Kidanemariam, A., Dagnew, A., Antonellini, M., 2021. Evolution of salinity and water table level of the phreatic coastal aquifer of the Emilia Romagna region (Italy). Water 13, 372. https://doi.org/10.3390/w13030372.
Giustiniani, M., Busetti, M., Dal Cin, M., Barison, E., Cimolino, A., Brancatelli, G., Baradello, L., 2022. Geophysical and geological views of potential water resources in the north-eastern Adriatic Sea. Geosciences 12, 139. https://doi.org/10.3390/geosciences12030139.
Gustafson, C., Key, K., Evans, R.L., 2019. Aquifer systems extending far offshore on the U.S. Atlantic Margin. Sci. Rep. 9, 8709. https://doi.org/10.1038/s41598-019-44611-7.
Haroon, A., Micallef, A., Jegen, M., Schwalenberg, K., Karstens, J., Berndt, C., Garcia, X., Kühn, M., Rizzo, E., Fusi, N.C., 2021. Electrical resistivity anomalies offshore a carbonate coastline: evidence for freshened groundwater? Geophys. Res. Lett. 48, e2020GL091909. https://doi.org/10.1029/2020GL091909.
Hathaway, J.C., Poag, C.W., Valentine, P.C., Manheim, F.T., Kohout, F.A., Bothner, M.H., Miller, R.E., Schultz, D.M., Sangray, D.A., 1979. US Geological Survey core drilling on the Atlantic shelf: geologic data were obtained at drill-core sites along the eastern US continental shelf and slope. Science 206, 515–527. https://doi.org/10.1126/science.206.4418.515.
Hawkins, P.J., 1972. Carboniferous sandstone oil reservoirs, East Midlands, England. Ph.D thesis, University of London.
Horozal, S., Micallef, A., De Biase, M., Chidichimo, F., 2025. Geological and sea level controls on offshore freshened groundwater in a rift basin: Gulf of Corinth, Greece. Hydrogeol. J. https://doi.org/10.1007/s10040-025-02943-x (in press).
Jiao, J.J., Shi, L., Kuang, X., Ming Lee, C., Yim, W.W.S., Yang, S., 2015. Reconstructed chloride concentration profiles below the seabed in Hong Kong (China) and their implications for offshore groundwater resources. Hydrogeol. J. 23, 277–286. https://doi.org/10.1007/s10040-014-1201-6.
Lambeck, K., Rouby, H., Purcell, A., Sun, Y., Sambridge, M., 2014. Sea level and global ice volumes from the Last Glacial Maximum to the Holocene. Proc. Natl. Acad. Sci. USA 111, 15296–15303. https://doi.org/10.1073/pnas.1411762111.
Levantesi, S., 2022. Italy must prepare for a future of chronic drought. Nature Italy, 14 July 2022. https://doi.org/10.1038/d43978-022-00089-y.
Lipparini, L., Chiacchieri, D., Bencini, R., Micallef, A., 2023. Extensive freshened groundwater resources emplaced during the Messinian sea-level drawdown in southern Sicily, Italy. Commun. Earth Environ. 4, 430. https://doi.org/10.1038/s43247-023-01077-w.
Lobo, F.J., Ridente, D., 2014. Stratigraphic architecture and spatio-temporal variability of high-frequency (Milankovitch) depositional cycles on modern continental margins: an overview. Mar. Geol. 352, 215–247. https://doi.org/10.1016/j.margeo.2013.10.009.
Lofi, J., Inwood, J., Proust, J.N., Monteverde, D.H., Loggia, D., Basile, C., Otsuka, H., Hayashi, T., Stadler, S., Mottl, M.J., Fehr, A., 2013a. Fresh-water and salt-water distribution in passive margin sediments: insights from Integrated Ocean Drilling Program Expedition 313 on the New Jersey Margin. Geosphere 9, 1009–1024. https://doi.org/10.1130/GES00855.1.
Lofi, J., Pezard, P., Bouchette, F., Raynal, O., Sabatier, P., Denchik, N., Levannier, A., Dezileau, L., Certain, R., 2013b. Integrated onshore-offshore investigation of a Mediterranean layered coastal aquifer. Groundwater 51, 550–561. https://doi.org/10.1111/j.1745-6584.2012.01011.x.
Maselli, V., Hutton, E.W., Kettner, A.J., Syvitski, J.P., Trincardi, F., 2011. High-frequency sea level and sediment supply fluctuations during termination I: an integrated sequence-stratigraphy and modeling approach from the Adriatic Sea (Central Mediterranean). Mar. Geol. 287, 54–70. https://doi.org/10.1016/j.margeo.2011.06.012.
Massari, F., Rio, D., Barbero, R.S., Asioli, A., Capraro, L., Fornaciari, E., Vergerio, P.P., 2004. The environment of Venice area in the past two million years. Palaeogeogr. Palaeoclimatol. Palaeoecol. 202, 273–308. https://doi.org/10.1016/S0031-0182(03)00640-0.
Mastrocicco, M., Busico, G., Colombani, N., Vigliotti, M., Ruberti, D., 2019. Modelling actual and future seawater intrusion in the Variconi coastal wetland (Italy) due to climate and landscape changes. Water 11, 1502. https://doi.org/10.3390/w11071502.
Miall, A.D., 2013. The Geology of Fluvial Deposits: Sedimentary Facies, Basin Analysis, and Petroleum Geology. Springer, Berlin, Heidelberg, 582 p.
Micallef, A., Person, M., Haroon, A., Weymer, B.A., Jegen, M., Schwalenberg, K., Faghih, Z., Duan, S., Cohen, D., Mountjoy, J.J., 2020. 3D characterisation and quantification of an offshore freshened groundwater system in the Canterbury Bight. Nat. Commun. 11, 1372. https://doi.org/10.1038/s41467-020-14770-7.
Micallef, A., Person, M., Berndt, C., Bertoni, C., Cohen, D., Dugan, B., Evans, R., Haroon, A., Hensen, C., Jegen, M., 2021. Offshore freshened groundwater in continental margins. Rev. Geophys. 59, e2020RG000706. https://doi.org/10.1029/2020RG000706.
Mitchum, R.M., Jr., Vail, P.R., Thompson, S., III, 1977. Seismic Stratigraphy and Global Changes of Sea Level: Part 2. The Depositional Sequence as a Basic Unit for Stratigraphic Analysis. In: Payton, C.E. (Ed.), Seismic Stratigraphy — Applications to Hydrocarbon Exploration, 26. AAPG Mem., pp. 53–62. https://doi.org/10.1306/M26490C4.
Monegato, G., Ravazzi, C., Donegana, M., Pini, R., Calderoni, G., Wick, L., 2007. Evidence of a two-fold glacial advance during the last glacial maximum in the

Tagliamento end moraine system (eastern Alps). Quat. Res. 68, 284–302. https://doi.org/10.1016/j.yqres.2007.07.002.
Mountain, G.S., Proust, J.N., McInroy, D., 2009. New Jersey Shallow Shelf: Shallow water drilling of the New Jersey continental shelf: global sea level and architecture of passive margin sediments. Int. Ocean Drill. Program Sci. Prospectus 313, 55. https://doi.org/10.2204/iodp.sp.313.2009.
Muttoni, G., Carcano, C., Garzanti, E., Ghielmi, M., Piccin, A., Pini, R., Rogledi, S., Sciunnach, D., 2003. Onset of major Pleistocene glaciations in the Alps. Geology 31, 989–992. https://doi.org/10.1130/G19445.1.
Neal, J.E., Abreu, V., Bohacs, K.M., Feldman, H.R., Pederson, K.H., 2016. Accommodation succession (δA/δS) sequence stratigraphy: observational method, utility and insights into sequence boundary formation. J. Geol. Soc. 173, 803–816. https://doi.org/10.1144/jgs2015-165.
Nesci, O., Savelli, D., Troiani, F., 2010. Late-Quaternary alluvial fans in the northern Marche Apennines: implications of climate changes. Alp. Mediterr. Quat. 23, 145–156.
Nichols, G.J., Fisher, J.A., 2007. Processes, facies and architecture of fluvial distributary system deposits. Sediment. Geol. 195, 75–90. https://doi.org/10.1016/j.sedgeo.2006.07.004.
Nowroozi, A.A., Horrocks, S.B., Henderson, P., 1999. Saltwater intrusion into the freshwater aquifer in the eastern shore of Virginia: a reconnaissance electrical resistivity survey. J. Appl. Geophys. 42, 1–22. https://doi.org/10.1016/S0926-9851(99)00004-X.
Ori, G.G., 1993. Continental depositional systems of the Quaternary of the Po Plain (northern Italy). Sediment. Geol. 83, 1–14. https://doi.org/10.1016/S0037-0738(10)80001-6.
Ori, G.G., Friend, P.F., 1984. Sedimentary basins formed and carried piggyback on active thrust sheets. Geology 12, 475–478.
Oude Essink, G.H.P., 2000. Density dependent groundwater flow: salt water intrusion and heat transport. Lecture Notes Hydrol. Transport Processes/Groundwater Modelling II, 120 p.
Pascale, S., Ragone, F., 2025. Widespread multi-year droughts in Italy: identification and causes of development. Int. J. Climatol. 45, e8827.
Pellegrini, C., Bohacs, K.M., Drexler, T.M., Gamberi, F., Rovere, M., Trincardi, F., 2017a. Identifying the sequence boundary in over- and under-supplied contexts: the case of the late Pleistocene Adriatic continental margin. In: Hart, B., Rosen, N.C., West, D., D' Agostino, A., Messina, C., Hoffman, M., Wild, R., (Eds.), Sequence Stratigraphy: The Future Defined. SEPM Society for Sedimentary Geology, Vol. 36.
Pellegrini, C., Maselli, V., Cattaneo, A., Piva, A., Ceregato, A., Trincardi, F., 2015. Anatomy of a compound delta from the post-glacial transgressive record in the Adriatic Sea. Mar. Geol. 362, 43–59. https://doi.org/10.1016/j.margeo.2015.01.010.
Pellegrini, C., Maselli, V., Gamberi, F., Asioli, A., Bohacs, K.M., Drexler, T.M., Trincardi, F., 2017b. How to make a 350-m-thick lowstand systems tract in 17,000 years: the late Pleistocene Po River (Italy) lowstand wedge. Geology 45, 327–330. https://doi.org/10.1130/G38848.1.
Pellegrini, C., Asioli, A., Bohacs, K.M., Drexler, T.M., Feldman, H.R., Sweet, M.L., Maselli, V., Rovere, M., Gamberi, F., Dalla Valle, G., Trincardi, F., 2018. The late Pleistocene Po River lowstand wedge in the Adriatic Sea: controls on architecture variability and sediment partitioning. Mar. Petrol. Geol. 96, 16–50. https://doi.org/10.1016/j.marpetgeo.2018.03.002.
Perini, L., Calabrese, L., 2010. Il sistema mare-costa dell'Emilia-Romagna. Vol. 20. Edizioni Pendragon (in Italian).
Person, M., Defoor, W., Camille, A., Key, K., Evans, R., Dugan, B., Noyes, C., McIntosh, J., Solomon, D.K., Micallef, A., Willett, M., 2025. Testing different scenarios of freshwater emplacement on the New England continental shelf using hydrologic modeling constrained by electromagnetic, isotopic, and salinity data. Geol. Soc. Am. Bull. 137 (9-10), 3905–3922. https://doi.org/10.1130/B37466.1.
Person, M., Key, K., Steckler, M., Paola, C., Voller, V., Stadler, S., Micallef, A., Grall, C., Gustafson, C., Evans, R., Wilson, J., 2018. The role of sediment transport and sea-level fluctuations on the sequestration of offshore freshwater in passive continental margin environments. In: EGU Gen. Ass. Conf. Abstracts, p. 2619.
Petracchini, L., Tavani, S., Brandano, M., Carminati, E., Chiarabba, C., Conti, A., Devoti, R., Galli, P., Palano, M., Pezzo, G., Scognamiglio, L., 2025. Thrust fault maturity and coseismic behavior: insights from the 2022 Mw 5.8 Adriatic offshore earthquake. Earth Planet. Sci. Lett. 669, 119591. https://doi.org/10.1016/j.epsl.2025.119591.
Pieri, M., Groppi, G., 1981. Subsurface geological structure of the Po Plain, Italy. In: Progetto Finalizzato Geodinamica, 414. C.N.R. (Publ.), Roma, pp. 1-23.
Post, V.E.A., Groen, J., Kooi, H., Person, M., Ge, S., Edmunds, W.M., 2013. Offshore fresh groundwater reserves as a global phenomenon. Nature 504, 71–78. https://doi.org/10.1038/nature12858.
Regione Emilia-Romagna, Eni-Agip, 1998. Riserve Idriche Sotterranee della Regione Emilia-Romagna. In: Di Dio, G. (Ed.), Società Elaborazioni Cartografiche. Firenze. 119 pp. (in Italian).
Regione Lombardia, Eni-Divisione Agip, 2002. Geologia degli acquiferi padani della Regione Lombardia. In: Carcano, C., Piccin, A. (Eds.), Società Elaborazioni Cartografiche. Firenze, 130 pp (in Italian).
Ricci Lucchi, F., 1986. The Oligocene to recent foreland basins of the northern Apennines. In: Allen, P.A., Homewood, P. (Eds.), Foreland Basins, 8. I.A.S. Spec. Publ., pp. 105-139.
Ridente, D., Trincardi, F., Piva, A., Asioli, A., Cattaneo, A., 2008. Sedimentary response to climate and sea level changes during the past ~400 ka from borehole PRAD1-2 (Adriatic margin). Geochem. Geophys. Geosyst. 9, Q09007. https://doi.org/10.1029/2007GC001783.
Ridente, D., Trincardi, F., Piva, A., Asioli, A., 2009. The combined effect of sea level and supply during Milankovitch cyclicity: evidence from shallow-marine $\delta^{18}O$ records and sequence architecture (Adriatic margin). Geology 37, 1003–1006. https://doi.org/10.1130/G25730A.1.
Rider, M.H., Kennedy, M., 2011. The Geological Interpretation of Well Logs, 3rd Ed. Rider-French, 432 pp.
Ripa, G., Pitoni, E., 2001. March. Sand control experience in the Adriatic Sea. In: Offshore Mediterranean Conference and Exhibition, OMC-2001.
Rossi, M., Minervini, M., Ghielmi, M., Rogledi, S., 2015. Messinian and Pliocene erosional surfaces in the Po Plain-Adriatic Basin: insights from \allostratigraphy and sequence stratigraphy in assessing play concepts related to accommodation and gateway turnarounds in tectonically active margins. Mar. Petrol. Geol. 66, 192–216. https://doi.org/10.1016/j.marpetgeo.2014.12.012.
Scardia, G., Muttoni, G., Sciunnach, D., 2006. Subsurface magnetostratigraphy of Pleistocene sediments from the Po Plain (Italy): constraints on rates of sedimentation and rock uplift. Geol. Soc. Am. Bull. 118, 1299–1312. https://doi.org/10.1130/B25869.1.
Schlumberger, 1989. Log Interpretation: Principles and Applications. Schlumberger Educational Services, 240 pp.
Severi, P., Bonzi, L., Ferrari, V., Pellegrino, I., 2014. Managed aquifer recharge in the Marecchia alluvial fan (Rimini-Italy), start of the test and first results. Acque-Sotterranee Ital. J. Groundwater 3 (3), 49–54. https://doi.org/10.7343/as-083-14-0110.
Sheng, C., Jiao, J.J., Luo, X., Zuo, J., Jia, L., Cao, J., 2023. Offshore freshened groundwater in the Pearl River estuary and shelf as a significant water resource. Nat. Commun. 14, 3781. https://doi.org/10.1038/s41467-023-39507-0.
Sømme, T.O., Helland-Hansen, W., Martinsen, O.J., Thurmond, J.B., 2009. Relationships between morphological and sedimentological parameters in source-to-sink systems: a basis for predicting semi-quantitative characteristics in subsurface systems. Basin Res. 21, 361–387. https://doi.org/10.1111/j.1365-2117.2009.00397.x.
Spano, D., Armiento, M., Aslam, M.F., Bacciu, V., Bigano, A., Bosello, F., Breil, M., Buonocore, M., Butenschön, M., Cadau, M., Cogo, E., Colelli, F.P., Costa Saura, J.M., Dasgupta, S., De Cian, E., Debolini, M., Didevarasl, A., Ellena, M., Galluccio, G., Harris, R., Johnson, K., Libert, A., Lo Cascio, M., Lovato, T., Marras, S., Masina, S., Mercogliano, P., Mereu, V., Mysiak, J., Noce, S., Papa, C., Phelan, A.S., Pregagnoli, C., Reder, A., Ribotta, C., Sano, M., Santini, A., Santini, M., Sartori, N., Sini, E., Sirca, C., Tharmananthan, R., Torresan, S., Trabucco, A., 2021. G20 Climate Risk Atlas: impacts, policy and economics in the G20. Centro Euro-Mediterraneo Sui Cambiamenti Climatici (CMCC). https://doi.org/10.25424/cmcc/g20_climaterisk.
Storms, J.E., Weltje, G.J., Terra, G.J., Cattaneo, A., Trincardi, F., 2008. Coastal dynamics under conditions of rapid sea-level rise: Late Pleistocene to Early Holocene evolution of barrier–lagoon systems on the northern Adriatic shelf (Italy). Quat. Sci. Rev. 27, 1107–1123. https://doi.org/10.1016/j.quascirev.2008.02.009.
Teatini, P., Tosi, L., Strozzi, T., 2011. Quantitative evidence that compaction of Holocene sediments drives the present land subsidence of the Po Delta. Italy. J. Geophys. Res. Solid Earth 116, B08408. https://doi.org/10.1029/2010JB008122.
Toreti, A., Bavera, D., Acosta, N.J., Arias-Muñoz, C., Barbosa, P., De, J.A., Di, C.C., Fioravanti, G., Grimaldi, S., Hrast, E.A., Maetens, W., 2023. Drought in western Mediterranean – GDO analytical report – May 2023. Publications Office of the European Union, Luxembourg, 1-22 pp. doi:10.2760/883951.
Tosi, L., Zecchin, M., Franchi, F., Bergamasco, A., Da Lio, C., Baradello, L., Mazzoli, C., Montagna, P., Taviani, M., Tagliapietra, D., Carol, E., Franceschini, G., Giovanardi, O., Donnici, S., 2017. Paleochannel and beach-bar palimpsest topography as initial substrate for coralligenous buildups offshore Venice, Italy. Sci. Rep. 7, 1321. https://doi.org/10.1038/s41598-017-01483-z.
UN-Water, U.N., 2020. UN-Water Analytical Brief on Unconventional Water Resources. United Nations, Geneva, Switzerland. https://www.unwater.org/app/uploads/2020/08/UN-Water-Analytical-Brief-on-Unconventional-Water-Resources.pdf.
Vail, P.R., Mitchum Jr., R.M., Thompson, S. III, 1977. Seismic stratigraphy and global changes of sea level, Part 4: global cycles of relative changes of sea level. In: Payton, C.E. (Ed.), Seismic Stratigraphy—Applications to Hydrocarbon Exploration. AAPG Mem. 26, 83–97. doi:10.1306/M26490C6.
Valente, M., Del Prete, C., Facci, G., Martino, A., Grilli, G.R., Bravi, F., Reno, C., Ragazzoni, L., 2025. The 2023 floods in the Emilia-Romagna Region, Italy: a retrospective qualitative investigation into response strategies and criticalities. Int. J. Disaster Risk Reduct. 116, 105089. https://doi.org/10.1016/j.ijdrr.2024.105089.
van Geldern, R., Hayashi, T., Bottcher, M.E., Mottl, M., Barth, J.A.C., Stadler, S., 2013. Stable isotope geochemistry of pore waters and marine sediments from the New Jersey shelf: methane formation and fluid origin. Geosphere 9, 96–112. https://doi.org/10.1130/GES00859.1.
Vandenberghe, J., 2003. Climate forcing of fluvial system development: an evolution of ideas. Quat. Sci. Rev. 22, 2053–2060. https://doi.org/10.1016/S0277-3791(03)00213-0.

Voutchkov, N., 2018. Energy use for membrane seawater desalination—current status and trends. Desalination 431, 2–14. https://doi.org/10.1016/j.desal.2017.10.033.

Zamrsky, D., van Lith, J.J.H., van Beek, R., 2024b. Conceptual 3D groundwater models of offshore freshened groundwater extraction and its economic viability assessment. EGU Gen. Assem., Vienna, Austria, 14–19 Apr 2024, EGU24-10761. doi:10.5194/egusphere-egu24-10761.

Zamrsky, D., Oude Essink, G.H., Sutanudjaja, E.H., Van Beek, L.P.H., Bierkens, M.F., 2022. Offshore fresh groundwater in coastal unconsolidated sediment systems as a potential fresh water source in the 21st century. Environ. Res. Lett. 17, 014021. https://doi.org/10.1088/1748-9326/ac4073.

Zamrsky, D., Oude Essink, G.H., Bierkens, M.F., 2024. Global impact of sea level rise on coastal fresh groundwater resources. Earth's Future 12, e2023EF003581. https://doi.org/10.1029/2023EF003581.

Zecchin, M., Donda, F., Forlin, E., 2017. Genesis of the northern Adriatic Sea (northern Italy) since early Pliocene. Mar. Petrol. Geol. 79, 108–130. https://doi.org/10.1016/j.marpetgeo.2016.11.009.

Zecchin, M., Busetti, M., Donda, F., Dal Cin, M., Zgur, F., Brancatelli, G., 2022. Plio-Quaternary sequences and tectonic events in the northern Adriatic Sea (northern Italy). Mar. Petrol. Geol. 142, 105745. https://doi.org/10.1016/j.marpetgeo.2022.105745.